Structural and biochemical features of OXA-517: a Carbapenem and expanded-spectrum Cephalosporin hydrolyzing OXA-48 variant

Laura Dabos, Joanna Raczynska, Pierre Bogaerts, Agustin Zavala, Delphine Girlich, Remy Bonnin, Laurent Dortet, Aurélie Peyrat, Pascal Retailleau, Bogdan Iorga, et al.

Structural and biochemical features of OXA-517: a carbapenem and expanded-spectrum cephalosporin hydrolyzing OXA-48 variant.

Laura Dabos[1,2], Joanna E. Raczynska[3], Pierre Bogaerts[5], Agustin Zavala[6], Delphine Girlich[1,2], Remy A. Bonnin[1,2], Laurent Dortet[1,2,4], Aurélie Peyrat[1], Pascal Retailleau[6], Bogdan I. Iorga[6], Mariusz Jaskólski[3,7], Youri Glupczynski[5], Thierry Naas[1,2,4*]

[1] Team "Resist" UMR1184, INSERM, CEA, University Paris-Saclay, LabEx LERMIT, Faculty of Medicine, Le Kremlin-Bicêtre, France.

[2] French National Reference Center for Antibiotic Resistance: Carbapenemase-producing Enterobacterales, Le Kremlin-Bicêtre, France:

[3] Center for Biocrystallographic Research, Institute of Bioorganic Chemistry, Polish Academy of Sciences, Poznan, Poland.

[4] Department of Bacteriology-Hygiene, Bicêtre Hospital, APHP Paris-Saclay, Le Kremlin-Bicêtre, France

[5] Laboratory of clinical microbiology, National reference center for monitoring antimicrobial resistance in Gram-negative bacteria, CHU UCL Namur, Yvoir, Belgium.

[6] Université Paris-Saclay, CNRS UPR 2301, Institut de Chimie des Substances Naturelles, Labex LERMIT, Gif-sur-Yvette, France.

[7] Department of Crystallography, Faculty of Chemistry, A. Mickiewicz University, Poznan, Poland.

Abstract: 203; Manuscript: 6474

Tables: 3; Figures: 6

Supplemental material: Clinical case, and 2 Figures

Running title: OXA-517, an extended-spectrum OXA-48-variant

Keywords: oxacillinase, extended-spectrum β-lactamase, carbapenem, cephalosporin, hydrolysis, antibiotic resistance

* Corresponding author's address: Service de Bactériologie-Virologie, Hôpital de Bicêtre, 78 rue du Général Leclerc 94275 Le Kremlin-Bicêtre Cedex, France. Phone: +33 1 45 21 29 86. Fax: +33 1 45 21 63 40. E-mail: thierry.naas@aphp.fr

Abstract (203)

OXA-48-producing Enterobacterales have now widely disseminated throughout the world. Several variants have now been reported, differing by just a few amino-acid substitutions or deletions, mostly in the region of the loop β5-β6. As OXA-48 hydrolyzes carbapenems but lacks significant expanded-spectrum cephalosporin (ESC) hydrolytic activity, ESCs were suggested as a therapeutic option. Here, we have characterized OXA-517, a natural variant of OXA-48- with an Arg214Lys substitution and a deletion of Ile215 and Glu216 in the β5-β6 loop, capable of hydrolyzing at the same time ESC and carbapenems. MICs values of *E. coli* expressing $bla_{\text{OXA-517}}$ gene revealed reduced susceptibility to carbapenems (similarly to OXA-48) and resistance to ESCs. Steady state kinetic parameters revealed high catalytic efficiencies for ESCs and carbapenems. The $bla_{\text{OXA-517}}$ gene was located on a ca. 31-kb plasmid identical to the prototypical IncL $bla_{\text{OXA-48}}$-carrying plasmid except for an IS*1R*-mediated deletion of 30.7-kb in the *tra* operon. The crystal structure of OXA-517, determined to 1.86 Å resolution, revealed an expanded active site as compared to that of OXA-48, which allows for accommodation of the bulky ceftazidime substrate. Our work illustrates the remarkable propensity of OXA-48-like carbapenemases to evolve through mutation/deletion in the β5-β6 loop to extend its hydrolysis profile to encompass most ß-lactam substrates.

Introduction

Antimicrobial resistance is the most alarming problem that is emerging in infectious diseases. β-Lactams, due to their safety, reliable killing properties and clinical efficacy, are among the most frequently prescribed antibiotics used to treat bacterial infections. However, their utility is being threatened by the worldwide proliferation of β-lactamases (BLs) with broad hydrolytic capabilities (1). Currently, BL-mediated resistance does not spare even the most powerful β-lactams (i.e. carbapenems), whose activity is challenged by carbapenemases (1,2). OXA-48, a Carbapenem-Hydrolyzing class D β-Lactamase (CHDL) initially identified in a carbapenem-resistant *Klebsiella pneumoniae* isolate from Turkey in 2001, has now spread globally in Enterobacterales (3,4). Several variants have since been reported, differing by a few amino acid substitutions or deletions (5). For a complete list of variants see the Beta-Lactamase DataBase (6; http://bldb.eu/BLDB.php?class=D#OXA). OXA-48 hydrolyzes penicillins at a high level, carbapenems at a low level and lacks significant hydrolytic activity towards expanded-spectrum cephalosporin (ESC) (5). While some OXA-48-variants with single amino acid substitutions have similar hydrolytic profiles as OXA-48, others, such as OXA-163 or OXA-405, carry a four-amino-acid deletion that results in the loss of carbapenemase activity and a gain of the ability to hydrolyze expanded-spectrum cephalosporins (5, 7-9). A novel OXA-48-variant, OXA-438, with two AA deletions and four AA changes in the β5–β6 loop, has been described with increased ability to hydrolyze carbapenems and decreased inactivation of oxyimino-cephalosporins compared to OXA-163 (9,10). Finally, Dabos *et al.* has shown by introducing one to six amino-acids deletions in the β5–β6 loop in both directions, that loss of carbapenem-hydrolysis and gain of cephalosporin hydrolysis occurred after four-amino acid deletions (11).

The hydrolysis of β-lactam antibiotics by OXA-48 and other class D ß-lactamases (DBLs) proceeds via acylation and deacylation of the active-site serine and involves a carboxylated lysine

as the general base (12,13). This reversible lysine modification, which is essential for DBL-activity, is proposed to be a spontaneous reaction, facilitated by the hydrophobic environment of the active site, which favors the unprotonated state of the lysine, and on the availability of CO_2 (12,14,15).

Despite a remarkable sequence divergence with other DBLs, the tertiary structure of OXA-48 is very similar to that of other DBLs (16,17). One notorious difference is that the β5 and β6 strands, located close to the substrate binding site, are overall shorter in OXA-48 than in other DBLs. (16,17). Consequently, the β5–β6 loop has a different length and orientation from that found in other DBLs. The observed conformation of the loop in OXA-48 is promoted by a salt bridge of Arg214 with the Ω-loop Asp159 residue (16,18). The β5–β6 loop extends into the outer portion of the active site crevice and defines a rather hydrophilic cavity filled with several water molecules, one of which will perform the nucleophilic attack on the acyl-enzyme intermediate in the deacylation step (16,18).

In OXA-163 or OXA-405, OXA-48-like enzymes that hydrolyze expanded-spectrum cephalosporins instead of carbapenems, the β5−β6 loop is shorter due to a 4 AA deletion that results in an expanded active-site cavity compared to that of OXA-48 (8,19). Arg214 is within the four-amino acid deletion, which eliminates one boundary of the active site and elongates the groove. As Arg214 has been suggested to form electrostatic interactions with carbapenem substrates to facilitate their hydrolysis, this could explain the low activity of OXA-163 and OXA-405 toward carbapenems (8,18). Additionally, this expansion of the active site of OXA-163 and OXA-405 is consistent with the ability of the enzyme to accommodate a larger substrate such as ceftazidime (8,19). The hypothesis that Arg214 contributes to the inability of OXA-48 to accommodate ceftazidime is additionally supported by the observation that a shorter and

uncharged side chain at position 214 (Arg214Ser substitution) results in an increased ceftazidime hydrolysis activity by OXA-232, an OXA-48-like enzyme (18).

The aim of the present study was to characterize OXA-517, a novel OXA-48-variant capable of hydrolyzing carbapenems and expanded-spectrum cephalosporins, identified in a clinical *K. pneumoniae* isolate recovered in Belgium.

Results

Clinical case.

K. pneumoniae 1219 clinical isolate (*Kp* 1219) was recovered from culture of a sputum specimen of 81-year-old woman hospitalized in a Belgium hospital in September 2015 (Supplementary material). Antimicrobial therapy was initiated with temocillin and rapidly switched to piperacillin because of rapid alteration of the status and development of a severe septic shock with acute renal failure. The patient was admitted to the intensive care unit where she received several antimicrobial agents including meropenem followed by cefepime, colistin and tigecycline. After four weeks, *Kp* 1219 isolate was repeatedly isolated over the period from throat, sputum, tracheobronchial aspirates, and BAL (bronchoalveolar lavage) specimens of the patient.

Antimicrobial susceptibility testing of *Kp* 1219 and carbapenemase confirmation tests.

Using broth microdilution (Sensititre), *Kp* 1219 was resistant to amoxicillin and piperacillin (Table 1), expanded spectrum cephalosporins, and carbapenems, except for meropenem where we observed intermediate susceptibility (Table 1). In addition, the strain was resistant to colistin.

Biochemical tests based on imipenem hydrolysis (Carba NP and BYG Carba tests [20,21]) gave positive results. Although the resistance phenotype was compatible with the production of an OXA-48-like carbapenemase enzyme, the immunochromatographic OXA-48 K-SeT® assay (Coris

BioConcept) yielded a negative result. On the other hand, OXA-163 K-SeT®, that specifically detects the OXA-163 enzyme, and NG-Test Carba5 (NG Biotech) assays were positive for OXA-163 and OXA-48, respectively. Other commercially-available tests based on carbapenem-hydrolysis such as Maldi-TOF (Star BL, Brucker) and ß-Carba (BioRad) (22,23) or on phenotypic approaches such as CIM or rCIM (24,25) clearly identified this isolate as Carbapenemase-Producing Enterobacterales (CPE). Similarly, with an inoculum of 10^3 CFU, *K. pneumoniae* 1219 strain grew in ChromID® ESBL (BioMérieux) and on the CARBA side of ChromID® CARBA SMART (BioMérieux), but not on the OXA-48 side.

PCR and sequencing revealed the presence of a novel $bla_{\text{OXA-48}}$ allele, designated $bla_{\text{OXA-517}}$ gene. $bla_{\text{OXA-517}}$ gene differed from the $bla_{\text{OXA-48}}$ gene by a 6-bp deletion, which included 2 nucleotides of the codon coding for Arg214, the entire codon coding for Ile215 and one nucleotide of the codon coding for Glu216. With this deletion, a novel codon was created coding for a Lys214, while the Ile215 and Glu216 were deleted (Figure 1).

Genomic features of *K. pneumoniae* 1219

WGS sequencing of *Kp* 1219 revealed a genome of 5,339,000 bp with a mean coverage of 90.7 X. The Multi Locus Sequence Typing (MLST) *of Kp* 1219 according to MLST 1.8 software (26) (https://cge.cbs.dtu.dk/services/,) revealed ST-188 (3-1-1-3-4-28-39), an ST type rarely described in hospital settings associated with carbapenemase or ESBL genes (27,28).

The resistome was analyzed by searching acquired genes and point mutations involved in resistance (29). The naturally occurring $bla_{\text{SHV-37}}$ gene, the acquired $bla_{\text{TEM-1}}$ gene and the $bla_{\text{OXA-517}}$ carbapenemase gene, were identified in this isolate. *Kp* 1219 also contained an *aph(3')-Ic* gene conferring resistance to kanamycin and neomycin (30), *str*A and *str*B conferring resistance to streptomycin (31), *sul*1, *sul*2 genes conferring resistance to sulphonamides (32) and the

142 dihydrofolate reductase gene (*dfr*A14) conferring resistance to trimethoprim (33). In addition,
143 *oqxA* and *oqxB* genes were also present in the isolate, conferring reduced susceptibility to
144 fluoroquinolones (MIC of 0.5 μg/ml to ciprofloxacin) (34). *FosA* gene conferring resistance to
145 fosfomycin was also present in the genome (35).

146 According to PlasmidFinder (36), different plasmid replication origins belonging to the
147 incompatibility groups, IncFIB, IncX3, ColRNAI, IncL and IncFII were identified. The $bla_{\text{OXA-517}}$ gene
148 was carried by the IncL-type plasmid as described previously for the $bla_{\text{OXA-48-like}}$ carbapenemase
149 genes, except for $bla_{\text{OXA-181}}$ and $bla_{\text{OXA-232}}$ genes (37-39).

150

151 **Genetic support and environment of $bla_{\text{OXA-517}}$ gene**

152 The $bla_{\text{OXA-517}}$ gene was located on a Tn*1999* composite transposon (Fig. 2A), as described
153 for $bla_{\text{OXA-48}}$ gene (4). The pOXA-517 plasmid was identical to the prototypical pOXA-48 plasmid of
154 61,881-bp (38; accession number JN626286) except for a 31,488-bp deletion from nucleotide
155 31,191 to 21 according to the pOXA-48 plasmid numbering. This deletion includes *ssb* gene, *mobC*
156 and *mobA* genes; *nikB* and *nikA* genes, all the Locus *Tra*, and part of *excA* genes that were replaced
157 by an insertion sequence IS*1R* (Fig 2B). Transfer of the β-lactam resistance marker into *E. coli* J53
158 by mating-out experiments failed with pOXA-517, confirming that this deletion impacted the
159 transfer ability of pOXA-517. Electroporation of this plasmid into *E. coli* TOP10 yielded
160 transformants resistant to β-lactams including carbapenems.

161

162 **Phenotypical characterization of OXA-517 β-lactamase**

163 The comparison of antibiotic susceptibility profiles conferred by OXA-48, OXA-163, and
164 OXA-517 was performed by cloning the corresponding genes into pCR-Blunt II-Topo kit (Invitrogen)
165 and expressing them in *E. coli* TOP10 (Table 1). Unlike pTOPO-OXA-48, pTOPO-OXA-163 and

166 pTOPO-OXA-517 conferred similar resistance phenotype for ceftazidime (MIC 16 µg/mL and 4
167 µg/mL, respectively), conferred decreased susceptibility to aztreonam and an increased
168 susceptibility to temocillin (32 µg/mL). At the same time, pTOPO-OXA-517 conferred decreased
169 susceptibility to carbapenems similarly to pTOPO-OXA-48, with MIC value for imipenem of 0.38
170 µg/mL (Table 1).
171
172 **Biochemical properties of OXA-517**
173 Steady-state kinetics parameters were determined to compare the catalytic properties of
174 OXA-517 with those of OXA-48 and OXA-163. OXA-517 was purified in one step pseudo-affinity
175 chromatography using an NTA-Ni column. OXA-163 and OXA-48 were previously purified by
176 Oueslati *et al.* (5) and Docquier *et al.* (16) and the kinetic parameters determined previously for
177 these enzymes were used for comparison. The catalytic efficiency of OXA-517 for ceftazidime was
178 overall close to that observed for OXA-163 (2 $mM^{-1}s^{-1}$ and 3 $mM^{-1}s^{-1}$ respectively). Conversely,
179 OXA-48 was not capable of hydrolyzing ceftazidime (Table 2). OXA-517 had a catalytic activity for
180 imipenem ~250-fold higher in comparison with the one of OXA-163 and ~25-fold lower than that
181 of OXA-48 (Table 2). These results are in agreement with the obtained MIC values. OXA-517 had
182 poor affinity for temocillin, with K_m ~15-fold higher than that for OXA-48. Another notable
183 difference with OXA-48 and with OXA-163 concerns the behavior of OXA-517 with penicillins. The
184 addition of $NaHCO_3$ as a source of CO_2 did not change the profile of hydrolysis of these penicillins.
185 The catalytic efficiency of OXA-517 was ~9-fold lower than that of OXA-48 but ~4-fold higher than
186 that of OXA-163. These results correlate with the differences in enzymatic turnover, while the K_m
187 values are similar for all three enzymes (Table 2). Unlike OXA-48, OXA-517 was capable of
188 hydrolyzing aztreonam, with a catalytic efficiency similar to the one of OXA-163 (3.1 mM^{-1} s^{-1} and
189 2.0 mM^{-1} s^{-1}, respectively).

Inhibition studies by determining the IC_{50} values indicated that OXA-517 was more potently inhibited by clavulanic acid (14 µM) and tazobactam (2 µM) than OXA-48 (30 µM and 20 µM, respectively). However, the inhibition efficiency with NaCl was lower for OXA-517 as compared to OXA-48 (400mM and 35mM respectively).

Crystal structure of OXA-517

Four OXA-517 protein molecules are present in the asymmetric unit of the crystal, and they form two non-crystallographic dimers related by pseudo translation. Each dimer has a two-fold rotational symmetry, with the symmetry axis approximately parallel to the [110] direction. The electron density maps are of good quality with all four polypeptide chains clearly defined. Each subunit possesses a two-domain structure with a helix bundle domain and an α/β domain with a central seven-stranded antiparallel β-sheet, as described for OXA-48 (16) (Fig. 3). Compared to OXA-48, OXA-517 carries an Ile215-Glu216 deletion coupled with an Arg214Lys mutation in the functionally important β5-β6 loop. In OXA-517 the loop is comprised of residues Thr213, Lys214, Pro217 and Lys218 (residue numbering corresponding to OXA-48). All the backbone atoms within the loop are visible in the electron density map but are not well ordered as indicated by their high atomic displacement parameters (Fig. 3, Fig. 4). The side chain of Lys214 is not visible in the electron density in any of the protein molecules. The peptide bond between Lys214 and Pro217 has a *cis* configuration as observed in OXA-48. A neighboring loop (residues 241-246), connecting the β7 strand with helix α10, shows a similarly high mobility, with high average B values (Fig. 3).

The four protein molecules are nearly identical with rmsd values between 0.05 and 0.32 Å for their Cα superpositions. The largest deviations between the subunits are visible at the

213 N-terminus and within the loop between helices α3 and α4, which participates in crystal-lattice
214 interactions.
215
216 **Dimer interface**
217 The OXA-517 dimer interface is the same as in OXA-48. In each of the two dimers a sulfate
218 ion is bound between two Arg206 residues contributed by the dimer-forming subunits (Fig. 4A, B).
219 Refining the sulfate ions at full occupancy resulted in negative difference density peaks (Fig. 4C)
220 and poor electron density fit criteria. Refinement at 0.5 occupancy gives good fit to the electron
221 density but results in the appearance of a localized positive difference density peak in the position
222 right in the middle between the two arginine residues (Fig. 4D). Modeling a half-occupancy
223 chloride ion in this position resulted in clear electron density maps and realistic temperature
224 factors for both partially occupied anions (Fig. 4B). In the structures of OXA-48 (PDB id 4s2p) and
225 OXA-163 (4s2l) that we used for comparisons, a water molecule was modeled in this position.
226 However, in both cases the water had an unrealistically low temperature factors and we noted
227 positive difference density peaks. Refinement of a chloride ion gave good electron density fit with
228 no peaks in the difference map and B factors like those of the environment. We conclude that in
229 those two structures, a chloride ion is also bound at each dimer interface. The Arg206 residue that
230 interacts with the bound anions originates at the amino end of the β5 strand, opposite to the β5-
231 β6 loop.
232
233 **The active site**
234 The active site is located at the interface of the two domains, between helices α3, α5 and
235 α6, and the β5 strand. All the active site residues are well defined in the electron density map,
236 including the carboxylated Lys73 (KCX) residue. The Oγ atom of the catalytically important Ser70

nucleophile exhibits considerably higher B factor than its surroundings, except in chain B. The full hydrogen bond network within the active site area is shown in Fig. S1. The Oγ atom of Ser70 interacts with KCX73, with the hydroxyl group of Ser118 and with a water molecule bound between the amide NH groups of Ser70 and Tyr211 (the oxyanion hole). This water molecule also interacts with the main-chain carbonyl of Tyr211. A sulfate ion is bound in the active site in all the four protein subunits and forms an ionic interaction with Arg250. The orientation of this anion is different in each of the subunits. The sulfate ion forms hydrogen bonds with the Oγ1 atom of Thr209 and water in all chains, and with the Nζ atom of Lys208 in chains A, B and C. Only one water position within the active site is conserved between the four protein subunits.

Similarly, as in OXA-48, the walls of the active site cavity are lined by the Leu158 side chain and by residues in the β5 strand, Tyr211-Ser212-Thr213. The groove ends with a hydrophilic cap formed by Oγ1_Thr213, N_Thr213, Oγ_Ser212 and O_Leu158.

Comparison with OXA-48 and OXA-163

The molecular structure of OXA-517 aligns well with that of OXA-48 (PDB id 4s2p) with an average rmsd of 0.50 Å for 238 superposed Cα atoms, and with OXA-163 (4s2l) with an average rmsd of 0.28 Å for 237 Cα atoms (Fig. 5A). The total number of Cα atoms in the aligned chains was equal to 244 for OXA-517, 238 for OXA-163 and 243 for OXA-48. The largest differences between these structures are found in the β5-β6 loop, where each protein has a slightly different sequence. The seven-residue loop (with the sequence ^{212}STRIEPK) in OXA-48 is replaced by a shorter sequence (^{212}STKPK) in OXA-517, and shorter yet in OXA-163 (^{212}DTK). In OXA-48, Arg214 forms a salt bridge with Asp159. This arginine is replaced by Lys214 in OXA-517 but a similar interaction is not observed in the structure of OXA-517. The side chain of Lys214 itself is not visible in the electron density but the loop is considerably shorter and there is a 3.8 Å distance between the Cα

atoms of Arg214 and Lys214 in the superposed structures of OXA-48 and OXA-517. An interaction between Lys214 and Asp159 would not be possible without significant conformational changes in either the β5-β6 or the Ω loop. A common feature of the β5-β6 loop in OXA-48 and OXA-517 is a *cis* peptide bond preceding Pro217 and a similar backbone conformation of this residue, even though it has a different position and orientation (Fig. 5B). The side chain of Thr213 has a different orientation in the two structures with the Oγ1 atom in OXA-517 pointing more 'down' towards the bottom of the binding cleft (Fig. 5 C, D). The fragment of the loop with the most pronounced differences between these two structures is between Thr213 and Lys218. Before and after this region the backbone atoms align well with each other. This contrasts with the structure of OXA-163, where the main chain atoms on the side of the β5 strand only converge with the other two structures at the N atom of Asp212 (Fig. 5B, E). In OXA-517 and OXA-48 the carbonyl O atom of Ser212 forms a hydrogen bond with N_Ile219. The Asp212-Thr213 peptide bond in OXA-163 has a different conformation and there is no hydrogen bond with N_Ile219. The side chain of Asp212 in this protein folds towards the loop and interacts with N_Lys218. Also, the side chain of Tyr211 has a different position in OXA-163 compared with the other structures but the electron density for this residue is weak. The relevant details of these comparisons are illustrated in Fig. 5B-E.

Comparison with OXA-48 P68A mutant in complex with ceftazidime

No naturally occurring OXA-48-like enzyme has been crystallized with ceftazidime, but Frohlich et al (40) report the structure of ceftazidime in complex with the OXA-48 P68A mutant, obtained by directed evolution *in vitro* (PDB id 6q5f). In this complex they observe ceftazidime with its carboxypropyloxiimino substituent placed between Thr213 from the β5-β6 loop and Leu158 from the Ω loop, and the aminothiazole ring pointing outwards the active site cavity, towards the solvent. When aligned onto OXA-517, RMSD between 223 pruned atom pairs is 0.388 angstroms.

Main differences are observed in the conformation of the β5-β6 loop, as explained previously, as well as in the Ω loop, which seems to be highly disordered between Asp148 and Ile162 in the ceftazidime-bound structure and therefore not modelled. When aligning this structure on the OXA-48 native structure (PDB id 4s2p), numerous severe clashes with the β Carbon of Thr213 and the whole Arg214 residue occur, as well as complete superposition with Leu158 on the Ω loop (Fig. 6A). Frohlich et al. propose that ceftazidime can bind in their OXA-48 mutant because of the increased flexibility of its loops due to the P68A mutation (40). Instead, when aligned on the β5-β6 loop of OXA-517, only two clashes occur, with Thr213 atoms Oγ1 and Cγ2, which might be avoided by rotation of this sidechain (Fig. 6B). Regarding Leu158 on the Ω loop, severe clashes are observed here as well (Fig. 6B), which may suggest that the same mechanism proposed by Frohlich et al might be at play here (40). The β5-β6 loop mutations may render the Ω loop more flexible in OXA-517 (see below), possibly allowing ceftazidime to bind.

Comparison with OXA-48 and OXA-163 in complex with imipenem

Two OXA-48 structures in complex with imipenem (PDB id 6p97 by Smith *et al.* (41) and PDB id 7kh9 by Stojanoski *et al.* (42)) may also be used for comparison with OXA-517. Both structures show relevant catalytic site residues mostly acquiring the same conformation, as does the core and R2 substituent of imipenem. Only the R1 tail, which shows signs of flexibility in both cases, adopts a different orientation in these two structures. When aligning OXA-517 to these structures, RMSD between 238 pruned atom pairs is 0.366 angstroms for 6p97 and 0.423 angstroms for 7kh9. The main difference is in the orientation of the β5-β6 loop, as shown for the OXA-48 apo structure, and most residues around the binding pocket adopt virtually the same conformation (Fig. S2). It was proposed that, similar to other class D carbapenemases, OXA-48 is capable of hydrolyzing carbapenems such as imipenem because of a hydrophobic barrier formed by Leu158 on the Ω loop and Val120 on the α4-α5 loop that protects the carboxylated Lys73 from

exposure to bulk solvent, while still allowing inside the active site a water molecule that will be activated to attack the acyl-enzyme complex (41). These residues adopt the same orientations in the active site cavity of OXA-517, the highest displacement being observed for Leu158 (0.7 Å) towards the carbapenem R2 substituent (Fig. S2). Leu158 maintains nevertheless the same distance to Val120 as in the other structures. It was also proposed that tight binding of carbapenems in the active site cavity may play a role in restraining them in a catalytically competent conformation, as suggested by the fact that non-carbapenemase OXA-163 showcases a wider catalytic pocket which binds imipenem more loosely (42). As described before, the β5-β6 loop mutations in OXA-517 seem to cause this loop to move farther from the Ω loop, closer to the β7-α10 loop, and allow Tyr211 to shift 0.8-1.3 Å (Fig. S2), which would slightly broaden the active site. In OXA-48, the β5-β6 loop interacts tightly with the Ω loop and subjacent Leu67-Ala69 sequence (Fig. 7A): Tyr211 and Ser212 maintain multiple contacts with Ala69; Ser212, Arg214 and Ile215 all interact with Leu67, while the latter two also contact Leu158 and Asp159 on the Ω loop. In OXA-163, however, with the β5-β6 loop deletions and the Ser212Asp mutation, most of these interactions are lost, and only one contact is observed, between Asp212 Cβ and Ala69 (Fig. 7C). In contrast, in OXA-517, some of the interactions between the β5-β6 and Ω loops are indirectly maintained via the Leu67-Ala69 stretch: similar to OXA-48, Tyr211 and Ser212 maintain almost all their contacts to Ala69 and Leu67, while the latter is now also contacted by the backbone of Lys214 (Fig. 7B). The Leu67-Pro68-Ala69 stretch, in turn, packs tightly with residues 157-162 of the Ω loop, as illustrated for the OXA-48 structure (Fig. 7D). It is also possible that less contacts between the β5 strand and Ala69 may influence the flexibility of Ser70 and the stability of the acyl-enzyme complex in a catalytically competent conformation. Therefore, this active site cavity broadening and maintenance of indirect interactions between the β5-β6 and Ω loops may explain why, unlike OXA-48, OXA-517 has acquired the capacity to hydrolyze ceftazidime, albeit at the cost

of a diminished affinity for imipenem. On the other hand, the turnover rate of OXA-517 for imipenem is closer to that of OXA-48 than of OXA-163.

Discussion

In this study, we have characterized a novel OXA-48 variant, OXA-517, recovered from a clinical isolate of *K. pneumoniae* from Belgium. OXA-517 hydrolyzes both ESC and carbapenems. OXA-163 and OXA-405 have a four-residue deletion in the region from Tyr-211 to Pro-217 in the β5-β6 loop and hydrolyze ESC but not carbapenems (8,19), whereas the OXA-48-like variants that possess carbapenemase activity have only substitutions of some residues in the β5-β6 loop region but no deletions. It is worth noting that contrary to what was observed for the OXA-48 variants OXA-163 and OXA-405, OXA-517 displays a deletion of only two AA residues in the β5-β6 loop and this is sufficient to confer resistance to expanded-spectrum cephalosporins as well as carbapenems. This is yet another fact that supports the hypothesis that substrate specificity of class D oxacillinases with respect to CHDL resides, at least in part, in the length and amino acid composition of loop β5-β6 (16, 18,19,43). OXA-438, another OXA-48 variant with two AA deletions (Thr213, Arg214) in the β5-β6 loop but with additional 4 AA substitutions (Ser212Gly, Ile215Tyr, Glu216Asp, Pro217Thr), has the same length of loop as OXA-517 but with different hydrolytic properties: comparable imipenem hydrolysis, 10-fold higher cefotaxime hydrolysis, and no detectable ceftazidime hydrolysis as compared to OXA-48 (10).

Temocillin has been proposed as a marker for the detection of OXA-48-like carbapenemase-producing Enterobacterales (44). Indeed, a diameter <12 mm for temocillin on disk diffusion antibiograms suggests the presence of OXA-48-producers with high specificity (90%). OXA-517 producing *K. pneumoniae* was not able to grow on the OXA-48 side of chromID® CARBA SMART (BioMérieux) even though the diameter around temocillin was 12mm (data not shown),

corresponding to a MIC value of 192 µg/mL. Thus OXA-517, similarly to OXA-244 or OXA-232, challenges the role of temocillin as a screening marker of OXA-48-like enzymes with true carbapenemase activity (45,46).

The *bla*$_{OXA-517}$ gene was identified on a plasmid with the backbone like the IncL *bla*$_{OXA-48}$-bearing plasmid (pOXA-48) (38), with the difference of a deletion of ca. 31 kb including *ssb* gene, *mobC* and *mobA* genes, *nikB* and *nikA* genes, all Locus *Tra* and part of *excA* gene. In the pOXA-517 plasmid, this region was replaced by the insertion sequence IS*1R*. Since the deleted region includes several genes involved in the mobilization and conjugative process of plasmids, we assume that this genetic rearrangement has led to the abrogation of the conjugative properties of the pOXA-517 plasmid as compared to pOXA-48 and, indeed, pOXA-517 was not found to be self-conjugative. Consequently, we might hypothesize that the genetic rearrangement observed in the pOXA-517 plasmid could limit its dissemination.

Considering the ability of OXA-517 to hydrolyze expanded-spectrum cephalosporins, our findings are consistent with the conclusions drawn for OXA-163 that a larger active site cavity allows for the binding and hydrolysis of the bulky ceftazidime substrate (19). The expansion of the cavity results from shortening of the β5-β6 loop and the elimination of arginine at position 214. Arg214 in OXA-48 forms a salt bridge with Asp159 and occupies part of the binding cavity (16,18). Any movement of this residue to free up more space for substrate binding would involve breaking this ionic interaction. In OXA-517, position 214 is occupied by a lysine residue which does not form a similar contact. As the β5-β6 loop in OXA-517 is by two residues shorter, there is a 3.8 Å distance between the Cα atom positions of residue 214 in OXA-517 and in OXA-48, and a similar salt bridge interaction between Lys214 and Asp159 would require a drastic conformational change. The larger size of the cavity is also attributed to the length of the β5-β6 loop, which in OXA-517 and OXA-163

380 is shorter than in OXA-48. Finally, as proposed by Frohlich et al. for the P68A OXA-48 mutant (40),
381 it is also possible that in OXA-517, with its mutated β5-β6 loop and broken interactions with the Ω
382 loop, the latter becomes now more flexible and allow for more space in the active site cavity to
383 bind ceftazidime.

384 On the other hand, the structural basis for carbapenemase activity is elusive. Regarding
385 affinity, it is possible that the differences between the OXA-48 and OXA-517 sequences cause the
386 latter to showcase a looser cavity. For example, the Ile102 is slightly farther away from Tyr211, as
387 illustrated in Fig. S2. This can also be observed when comparing the apo OXA-48 structure with the
388 apo OXA-517 structure (data not shown). However, the side chain of this latter residue is not well
389 defined in the electron density and exhibits high mobility, as indicated by the high temperature
390 factors in the crystal structure of OXA-517, as well as in OXA-163 (pdb id 4s2l) and OXA-48 (4s2p).
391 Therefore, the observed differences in the conformation of this residue might not be significant.
392 Perhaps the native OXA-48 structure is fairly optimal for the binding of carbapenems, and any
393 alteration, such as those observed in OXA-517 and OXA-163, are enough to alter altogether the
394 size of the cavity and diminish its affinity for them. It is possible that the acylation reaction for
395 carbapenem antibiotics proceeds in the same way for these three OXA enzymes, and only the
396 deacylation step is considerably slower for OXA-163, possibly due to its larger β5-β6 loop
397 modification having deeper consequences in its catalytic cycle dynamics. The kinetic data reported
398 for OXA-163 (19) show that a reduced catalytic efficiency for carbapenems, compared to OXA-48,
399 is mainly caused by a decrease in the turnover rate, with unchanged K_m. However, other literature
400 data show that there is both an increase in the K_M value and a decrease in k_{cat} for the tested
401 carbapenem compounds (5). The creation of an unusually stable carbapenem acyl-enzyme
402 intermediate was described for OXA-10 (43). It was also suggested that some orientations of the

403 hydroxyethyl group may restrict access of the hydrolytic water molecule to the covalent
404 intermediate, and thus prevent deacylation.

405 A possible explanation for the differences in carbapenemase activity of these three
406 enzymes is that the β5-β6 loop undergoes conformational changes and moves closer to the
407 substrate, thus influencing its conformation during the hydrolysis reaction. Such a view has been
408 already proposed by Docquier *et al.* (16). In our OXA-517 crystal structure all the loop residues
409 have high temperature factors, suggesting high conformational freedom of this structural element,
410 in agreement with its proposed long-range movements. The *cis*-Pro217 residue that is present in
411 both OXA-517 and OXA-48, but not in OXA-163, enforces a specific backbone conformation that
412 cannot be adopted by any other residue. This may be an important aspect of the activity of these
413 enzymes towards carbapenems. Indeed, the sequence comparisons presented by De Luca et al.
414 (43) revealed the presence of a conserved PxxG sequence motif (residues 217–220 in OXA-48
415 numbering) in all class D carbapenemases, but not in other OXA-type enzymes. Further structural
416 and biochemical data would be needed to confirm the importance of the *cis*-Pro217 residue.
417 Another possibility, as depicted in Fig. 7, is that the β5-β6 loop in OXA-517, relatively more similar
418 to that of OXA-48 than that of OXA-163, allows it to conserve some of the dynamic properties of
419 the native OXA-48 catalytic machinery, thus allowing for the turnover rate for imipenem to remain
420 similar too.

421 Our crystal structure of OXA-517 shows that the dimer interface is stabilized by a chloride
422 or/and sulfate anions bound between two Arg206 residues from the neighboring subunits. In OXA-
423 10, the structurally equivalent His203 residue forms part of a metal ion binding site (47).
424 Interestingly, it has been shown that supplementation of the buffer with some transition metal
425 ions shifts the equilibrium in solution towards the dimeric form of this enzyme, which in turn

increases its activity. An attractive hypothesis suggests itself, that the evolutionary advantage of OXA-48-like proteins compared to OXA-10 is that their dimer formation is independent of metal cations and is instead stabilized by the abundantly present Cl^- ions.

Finally, our work illustrates the possibility for OXA-48 to extend its substrate specificity to include ESC by point mutations/deletions. This finding may have clinical consequences, as the increased use of ESC to treat infections caused by OXA-48-producing isolates, remaining susceptible to ESC, may lead to selection of OXA-163-like or OXA-517-like variants.

Materials and methods

Bacterial strains

Klebsiella pneumoniae 1219 was identified with matrix-assisted laser desorption ionization–time of flight (MALDI-TOF) mass spectrometry (MALDI, Biotyper CA system, Bruker Daltonics, Billerica, MA, USA). *Escherichia coli* TOP10 (Invitrogen, Saint-Aubin, France) and *E. coli* BL21 (DE3) (Novagen, VWR International, Fontenay-sous-Bois, France) were used for cloning experiments. Azide-resistant *E. coli* J53 was used for conjugation assays. *K. pneumoniae* 11978 and *K. pneumoniae* 6299 were used as reference strains for OXA-48 and OXA-163 cloning experiments, respectively (4,7).

Antimicrobial agents, susceptibility testing, and microbiological techniques

Antimicrobial susceptibilities were determined by disk diffusion and Minimal Inhibitory Concentration (MICs) and interpreted as previously described (48). *Kp* 1219 was plated in different chromogenic medias: chromID® ESBL and chromID® CARBA SMART (BioMérieux).

Biochemical and immunochromatographic detection of carbapenemase-producing *Enterobacterales*

Carbapenemase activity was investigated using the Carba NP test (20), RAPIDEC® CARBA NP (BioMérieux), β-CARBA™ Test (Bio-Rad) (23), Maldi-TOF (Star BL, Brucker, Bremen, Germany) (22), BYG test (21), or using phenotypic approaches such as CIM or rCIM (24,25) as previously described. The expression of a carbapenemase was investigated using OXA-48 K-SeT® and OXA-163 K-SeT® immunochromatographic assay (Coris BioConcept, Gembloux, Belgium) and NG-Test Carba 5 (NG Biotech, Guipry, France) as recommended by the manufacturers.

PCR, cloning experiments, and DNA sequencing

Whole-cell DNAs of *K. pneumoniae* 1219 and *K. pneumoniae* 11978 isolates were extracted using the QIAamp DNA mini kit (Qiagen, Courtaboeuf, France) and were used as templates for PCR as previously described (48). The amplicons obtained were then cloned into the pCR®-Blunt II-TOPO® plasmid (Invitrogen, Illkirch, France), as previously described (48). The recombinant pTOPO-OXA plasmids were electroporated into *E. coli* TOP10 cells; and selected on kanamycin (50 µg/ml) containing plates. The $bla_{\text{OXA-517}}$ gene fragment corresponding to the mature β-lactamase was cloned into the expression vector pET41b (+) (Novagen, VWR International, Fontenay-sous-Bois, France) as previously described (48). The recombinant plasmid pET41-OXA-517 was transformed into the chemically competent *E. coli* strain BL21 (DE3) (Novagen).

Recombinant plasmids were extracted using the Qiagen miniprep kit and both strands of the inserts were sequenced using M13 and T7 primers, with an automatic sequencer (ABI Prism 3100; Applied Biosystems, Les Ulis, France). The nucleotide sequences were analyzed using software available at the National Center for Biotechnology Information website (http://www.ncbi.nlm.nih.gov).

Whole genome sequencing (WGS)

Total DNA was extracted from colonies using the Ultraclean Microbial DNA Isolation Kit (MO BIO Laboratories, Carlsbad, CA, US) following the manufacturer's instructions. The DNA concentration and purity were controlled by a Qubit® 2.0 Fluorometer using the dsDNA HS and/or BR assay kit (Life technologies, Carlsbad, CA, US). The DNA library was prepared using the Nextera XT-v3 kit (Illumina, San Diego, CA, US) as previously described (48). De novo assembly was performed by CLC Genomics Workbench v 9.5.3 (Qiagen) after quality trimming (Qs ≥ 20) with word size 34. The acquired antimicrobial resistance genes were identified by uploading the assembled genomes to the Resfinder server v2.1 (http://cge.cbs.dtu.dk/services/ResFinder-2.1) (29). The Multi Locus Sequence Typing (MLST) and the identification of the different plasmids were also obtained by uploading the assembled genomes to the MLST 1.8 (26) and PlasmidFinder 1.3 (36) servers, respectively, available at https://cge.cbs.dtu.dk/services/.

Plasmid characterization and conjugation assay

Plasmid DNA of the clinical isolates *Kp* 1219 and *K. pneumoniae* 11978 were extracted using the Kieser method (49). The Kieser extract from both *K. pneumoniae* isolates were used to transform *E. coli* TOP10 strain by electroporation. The electroporants were plated on a TSA plate containing 100 µg/ml ampicillin. The presence $bla_{OXA-517}$ gene was sought by PCR as previously described (53). From the transformants harboring the $bla_{OXA-517}$ gene, plasmid DNA extraction was done using the Kieser's method and subsequently analyzed on 0.7% agarose gel stained with ethidium bromide. Plasmids of ca. 154, 66, 48, and 7 kb of *E. coli* NCTC 50192 were used as plasmid size markers (50).

Quantitative filter mating-out assay was performed as previously described (48), and transconjugants were selected with 100 µg/ml ampicillin and 100 µg/ml azide. Transfer

496 frequencies were calculated by dividing the number of transconjugants by the number of donor
497 cells.
498
499 **β-Lactamase purification**
500 An overnight culture of *E. coli* strain BL21 (DE3) harboring pET41b-OXA-517 was used to
501 inoculate 2 L of LB broth containing 50 µg/mL kanamycin. Expression of OXA-517 was induced
502 overnight at 25°C with 0.2 mM IPTG, as previously described (48). Cultures were centrifuged at
503 6000 g for 15 min and the pellets were resuspended in 10 mL of Buffer A (20 mM phosphate
504 buffer, 175 mM potassium sulfate (K_2SO_4), 40 mM imidazol, pH 7.4). The cells were disrupted by
505 sonication and bacterial debris was removed by two consecutive centrifugation steps. OXA-517
506 was purified in one step pseudo-affinity chromatography using an NTA-Ni column (GE Healthcare,
507 Les Ulis, France) as previously described (48). Protein purity was estimated by SDS-PAGE, pure
508 fractions were pooled and dialyzed against 20 mM Hepes, 50 mM K_2SO_4 buffer (pH 7.0) and
509 concentrated using Vivaspin® columns (GE Healthcare, Freiburg, Germany). Protein concentration
510 was determined by Bradford Protein assay (Bio-Rad) (51). OXA-163 and OXA-48 were previously
511 purified by Oueslati *et al.* (5) and Doquier *et al.* (16).
512
513 **Steady-state kinetic parameters**
514 Kinetic parameters of purified OXA-517 were determined at 30°C in 100 mM sodium
515 phosphate buffer (pH 7.0). The k_{cat} and K_m values were determined by analyzing hydrolysis of β-
516 lactams under initial-rate conditions with an ULTROSPEC 2000 model UV spectrophotometer (GE
517 Healthcare). Kinetic parameters were calculated using the Eadie–Hoffstee linearization of the
518 Michaelis–Menten equation, as previously described (54). The β-lactams were purchased from
519 Sigma–Aldrich (Saint-Quentin-Fallavier, France). Comparative activation of OXA-517 by CO_2 was

conducted by monitoring the rate of hydrolysis of penicillins in the same buffer supplemented with 50 mM sodium hydrogen carbonate ($NaHCO_3$) as the source of CO_2 (15,18). OXA-163 and OXA-48 kinetic parameters, used in the comparison, were previously determined by Oueslati *et al.* (5) and Doquier et al. (16).

Crystallization, X-ray data collection, structure refinement and analysis

A 27 mg/ml protein solution was used for crystallization screening with the NeXtal crystallization kit (Qiagen). Single crystals of OXA-517 grew in 0.1 M MES pH 6.5 and 20% (w/v) PEG10000. The diffraction data were collected at the SOLEIL PROXIMA II beamline equipped with an Eiger detector (Table 3). The images were processed and scaled with the *XDS* package (52,53) producing intensities merged in the $P2_1$ space group as output. The intensities were then converted to structure factor amplitudes with *Truncate* (54) from the *CCP4* program suite (55). An inspection of the Patterson map, calculated using the FFT algorithm implemented in *fftbig* (56) from the *CCP4* package, revealed a large non-origin peak at 0.5, 0, 0.5, indicating translational pseudosymmetry. The structure was solved by molecular replacement using *Phaser* (57) and taking advantage of the detected pseudo translation. The starting model was a single subunit of OXA-48 (PDB id 4s2p). The calculations gave a single solution with a Z-score of 15.4 for the translation function and a final LLG of 2405. No twinning was found by the *Phaser* twin detection algorithm (58), which corrects for translational NCS. An alternative solution, shifted by 0.25, 0, 0.25, was also tested but it gave significantly higher R factors. The *Achesym* server (59) was used to standardize the placement of the model inside the unit cell. Maximum-likelihood refinement was carried out in *Refmac5* (60), while model rebuilding and analysis was done in *Coot* (61). For validation of the final model, we used *Molprobity* (62) and the PDB validation server (63). The SSM

543 algorithm implemented in *Coot* was used for 3D superpositions of different models. Figures were
544 generated with *Pymol* (64).

545 For comparisons of our structure with other models, we downloaded their coordinates
546 and, when available, the corresponding electron density maps from the Uppsala Electron Density
547 Server (*EDS*) (65). For a few PDB models, we applied some minor adjustments to their coordinates
548 to improve the electron density fit or stereochemical parameters. We used the *CCP4* package for
549 conversions between file formats and *Truncate* to convert the intensities to structure factor
550 amplitudes, if necessary. For structure comparison, UCSF ChimeraX software was used (66).
551

552 **Nucleotide sequence and PDB accession numbers**

553 The nucleotide sequence of the $bla_{\text{OXA-517}}$ gene has been submitted to the EMBL/Genbank
554 nucleotide sequence database under the accession number KU878974. The nucleotide sequence
555 of plasmid pOXA-517 has been submitted also, under the accession number KY200950. The Whole
556 Genome Shotgun of Kp1219 has been deposited at the DDBJ/ENA/GenBank under the accession
557 code NXNM00000000. The version described in this paper is version NXNM01000000. Atomic
558 coordinates and structure factors for the crystal structure of OXA-517 have been deposited with
559 the Protein Data Bank (PDB) with the accession number 6HB8.
560

561 **Acknowledgments**

562 We acknowledge SOLEIL for provision of synchrotron radiation facilities (proposal ID
563 BAG20170782) in using PROXIMA beamlines. This work has also benefited from the I2BC
564 crystallization platform, supported by FRISBI ANR-10-INSB-05-01. This work was supported by the
565 Assistance Publique – Hôpitaux de Paris (AP-HP), the University Paris-Saclay, the Laboratory of

Excellence in Research on Medication and Innovative Therapeutics (LERMIT) supported by a grant from the French National Research Agency [ANR-10-LABX-33], the Joint Programming Initiative on Antimicrobial Resistance (JPIAMR) DesInMBL [ANR-14-JAMR-002], and DIM Malinf, Ile de France, for LD's PhD fellowship.

Conflict of interest

None to declare

References

1. Bonomo RA. 2017. β-Lactamases: A Focus on Current Challenges. Cold Spring Harb Perspect Med 7:a025239.
2. Bonomo RA, Burd EM, Conly J, Limbago BM, Poirel L, Segre JA, Westblade LF. 2018. Carbapenemase-Producing Organisms: A Global Scourge. Clin Infect Dis 66:1290-1297.
3. Poirel L, Heritier C, Tolun V, Nordmann P. 2004. Emergence of oxacillinase-mediated resistance to imipenem in *Klebsiella pneumoniae*. Antimicrob Agents Chemother 48:15–22.
4. Aubert D, Naas T, Héritier C, Poirel L, Nordmann P. 2006. Functional characterization of IS1999, an IS4 family element involved in mobilization and expression of beta-lactam resistance genes. J Bacteriol 188:6506-6514.
5. Oueslati S, Nordmann P, Poirel L. 2015. Heterogeneous hydrolytic features for OXA-48-like β-lactamases. J Antimicrob Chemother 70:1059-63.
6. Naas T, Oueslati S, Bonnin RA, Dabos ML., Zavala A, Dortet L, Retailleau P, Iorga BI. 2017. Beta-Lactamase DataBase (BLDB) - Structure and Function. J Enz Inh Med Chem 32:917-919.

7. Poirel L, Castanheira M, Carrer A, Rodriguez CP, Jones RN, Smayevsky J, Nordmann P. 2011. OXA-163, an OXA-48-related class D β-lactamase with extended activity toward expanded-spectrum cephalosporins. Antimicrob Agents Chemother 55:2546–2551.
8. Oueslati S, Retailleau P, Marchini L, Dortet L, Bonnin RA, Iorga BI, Naas T. 2019. Biochemical and Structural Characterization of OXA-405, an OXA-48 Variant with Extended-Spectrum β-Lactamase Activity. Microorganisms 8:24.
9. Dabos L, Oueslati S, Bernabeu S, Bonnin RA, Dortet L, Naas T. 2022. To Be or Not to Be an OXA-48 Carbapenemase. Microorganisms 10:258.
10. De Belder D, Ghiglione B, Pasteran F, de Mendieta JM, Corso A, Curto L, Di Bella A, Gutkind G, Gomez SA, Power P. 2020. Comparative Kinetic Analysis of OXA-438 with Related OXA-48-Type Carbapenem-Hydrolyzing Class D beta-Lactamases. ACS Infect Dis 6:3026-3033.
11. Dabos L, Bonnin R, Dortet L, Iorga B, Naas, T. 2016. Biochemical and structural investigation of the role of beta5-beta6 loop in substrate specificity of OXA-48–like enzymes. ECCMID Amsterdam, The Netherlands
12. Golemi D, Maveyraud L, Vakulenko S, Samama JP, Mobashery S. 2001. Critical involvement of a carbamylated lysine in catalytic function of class D β-lactamases. Proc Natl Acad Sci USA 98:14280−14285.
13. Li J, Cross JB, Vreven T, Meroueh SO, Mobashery S, Schlegel HB .2005. Lysine carboxylation in proteins: OXA-10 β-lactamase. Proteins 61: 246−257.
14. Leonard DA, Bonomo RA, Powers RA .2013. Class D β-lactamases: A reappraisal after five decades. Acc Chem Res 46: 2407−2415.
15. Baurin S, Vercheval L, Bouillenne F, Falzone C, Brans A, Jacquamet L, Ferrer JL, Sauvage E, Dehareng D, Frere JM, Charlier P, Galleni M, Kerff F. 2009. Critical role of tryptophan 154 for the activity and stability of class D β-lactamases. Biochemistry 48:11252−11263.

16. Docquier JD, Calderone V, De Luca F, Benvenuti M, Giuliani F, Bellucci L, Tafi A, Nordmann P, Botta M, Rossolini GM, Mangani S .2009. Crystal structure of the OXA-48 β-lactamase reveals mechanistic diversity among class D carbapenemases. Chem Biol 16:540–547.
17. Dabos L, Zavala A, Bonnin RA, Beckstein O, Retailleau P, Iorga BI, Naas T. 2020. Substrate Specificity of OXA-48 after β5-β6 Loop Replacement. ACS Infect Dis 6:1032-1043.
18. Oueslati S, Retailleau P, Marchini L, Berthault C, Dortet L, Bonnin RA, Iorga BI, Naas T. 2020. Role of Arginine 214 in the Substrate Specificity of OXA-48. Antimicrob Agents Chemother 64:e02329-19.
19. Stojanoski V, Chow DC, Fryszczyn B, Hu L, Nordmann P, Poirel L, Sankaran B, Prasad BV, Palzkill T. 2015. Structural basis for different substrate profiles of two closely related class D β-lactamases and their inhibition by halogens. Biochemistry 21:3370-3380.
20. Dortet L, Agathine A, Naas T, Cuzon G, Poirel L, Nordmann P. 2015. Evaluation of the RAPIDEC® CARBA NP, the Rapid CARB Screen® and the Carba NP test for biochemical detection of carbapenemase-producing Enterobacteriaceae. J Antimicrob Chemother 70:3014-22.
21. Bogaerts P, Oueslati S, Meunier D, Nonhoff C, Yunus S, Massart M, Denis O, Woodford N, Hopkins KL, Naas T, Dortet L, Huang TD, Glupczynski Y. 2017. Multicentre evaluation of the BYG Carba v2.0 test, a simplified electrochemical assay for the rapid laboratory detection of carbapenemase-producing *Enterobacteriaceae*. Sci Rep 7:9937.
22. Dortet L, Tandé D, de Briel D, Bernabeu S, Lasserre C, Gregorowicz G, Jousset AB, Naas T. 2018. MALDI-TOF for the rapid detection of carbapenemase-producing Enterobacteriaceae: comparison of the commercialized MBT STAR®-Carba IVD Kit with two in-house MALDI-TOF techniques and the RAPIDEC® CARBA NP. J Antimicrob Chemother 73:2352-2359.

636 23. Bernabeu S, Dortet L, Naas T. 2017. Evaluation of the β-CARBA™ test, a colorimetric test
637 for the rapid detection of carbapenemase activity in Gram-negative bacilli. J Antimicrob
638 Chemother 72:1646-1658.
639 24. Gauthier L, Bonnin RA, Dortet L, Naas T. 2017. Retrospective and prospective evaluation of
640 the Carbapenem inactivation method for the detection of carbapenemase-producing
641 Enterobacteriaceae. PLoS One 12:e0170769.
642 25. Muntean MM, Muntean AA, Gauthier L, Creton E, Cotellon G, Popa MI, Bonnin RA, Naas T.
643 2018. Evaluation of the rapid carbapenem inactivation method (rCIM): a phenotypic
644 screening test for carbapenemase-producing Enterobacteriaceae. J Antimicrob Chemother
645 73:900-908.
646 26. Larsen MV, Cosentino S, Rasmussen S, Friis C, Hasman H, Marvig RL, Jelsbak L, Sicheritz-
647 Pontén T, Ussery DW, Aarestrup FM, Lund O. 2012. Multilocus sequence typing of total-
648 genome-sequenced bacteria. J Clin Microbiol 50:1355-61.
649 27. Ewers C, Stamm I, Pfeifer Y, Wieler LH, Kopp PA, Schønning K, Prenger-Berninghoff E,
650 Scheufen S, Stolle I, Günther S, Bethe A. 2014. Clonal spread of highly successful ST15-CTX-
651 M-15 *Klebsiella pneumoniae* in companion animals and horses. J Antimicrob Chemother
652 69:2676-80.
653 28. Zhou K, Lokate M, Deurenberg RH, Tepper M, Arends JP, Raangs EG, Lo-Ten-Foe J,
654 Grundmann H, Rossen JW, Friedrich AW. 2016. Use of whole-genome sequencing to trace,
655 control and characterize the regional expansion of extended-spectrum β-lactamase
656 producing ST15 *Klebsiella pneumoniae*. Sci Rep 6:20840.
657 29. Zankari E, Hasman H, Cosentino S, Vestergaard M, Rasmussen S, Lund O, Aarestrup FM,
658 Larsen MV. 2012. Identification of acquired antimicrobial resistance genes. *J Antimicrob*
659 *Chemother* 67:2640-264.

30. Ramirez MS, Tolmasky ME. 2010. Aminoglycoside Modifying Enzymes. Drug Resist Updat 13:151–171.
31. Sundin GW. 2002. Distinct recent lineages of the strA- strB streptomycin-resistance genes in clinical and environmental bacteria. Curr Microbiol 45: 63-9.
32. Skold O. 2000. Sulfonamide resistance: mechanisms and trends. Drug Resist Updat 3:155-160.
33. Bossé JT, Li Y, Walker S, Atherton T, Fernandez Crespo R, Williamson SM, Rogers J, Chaudhuri RR, Weinert LA, Oshota O, Holden MT, Maskell DJ, Tucker AW, Wren BW, Rycroft AN, Langford PR BRaDP1T Consortium. 2015. Identification of dfrA14 in two distinct plasmids conferring trimethoprim resistance in Actinobacillus pleuropneumoniae. J Antimicrob Chemother 70:2217-22.
34. Rodríguez-Martínez JM, Díaz de Alba P, Briales A, Machuca J, Lossa M, Fernández-Cuenca F, Rodríguez Baño J, Martínez-Martínez L, Pascual Á. 2013. Contribution of OqxAB efflux pumps to quinolone resistance in extended-spectrum-β-lactamase-producing *Klebsiella pneumoniae*. J Antimicrob Chemother 68:68-73.
35. Fillgrove KL, Pakhomova S, Newcomer ME, Armstrong RN. 2003. Mechanistic diversity of fosfomycin resistance in pathogenic microorganisms. J Am Chem Soc 125:15730-15731.
36. Carattoli A, Zankari E, Garcia-Fernandez A, Voldby Larsen M, Lund O, Villa L, Møller Aarestrup F, Hasman H. 2014. *In silico* detection and typing of plasmids using PlasmidFinder and plasmid multilocus sequence typing. Antimicrob Agents Chemother 58: 3895-903.
37. Carattoli A, Seiffert SN, Schwendener S, Perreten V, Endimiani A. 2015. Differentiation of IncL and IncM Plasmids Associated with the Spread of Clinically Relevant Antimicrobial Resistance. PLoS One 10: e0123063.

684 38. Poirel L, Bonnin RA, Nordmann P. 2012. Genetic features of the widespread plasmid
685 coding for the carbapenemase OXA-48. Antimicrob Agents Chemother 56: 559–562.
686 39. Potron A, Rondinaud E, Poirel L, Belmonte O, Boyer S, Camiade S, Nordmann P. 2013.
687 Genetic and biochemical characterisation of OXA-232, a carbapenem-hydrolysing class D
688 β-lactamase from *Enterobacteriaceae*. Int J Antimicrob Agents 41: 325–329.
689 40. Fröhlich C, Sørum V, Thomassen AM, Johnsen PJ, Leiros HS, Samuelsen Ø. 2019. OXA-48-
690 Mediated Ceftazidime-Avibactam Resistance Is Associated with Evolutionary Trade-Offs.
691 mSphere 4: e00024-19.
692 41. Smith CA, Stewart NK, Toth M, Vakulenko SB. 2019. Structural Insights into the Mechanism
693 of Carbapenemase Activity of the OXA-48 β-Lactamase. Antimicrob Agents Chemother 63:
694 e01202-19.
695 42. Stojanoski V, Hu L, Sankaran B, Wang F, Tao P, Prasad BVV, Palzkill T. 2021. Mechanistic
696 Basis of OXA-48-like β-Lactamases' Hydrolysis of Carbapenems. ACS Infect Dis 7: 445-460.
697 43. De Luca F, Benvenuti M, Carboni F, Pozzi C, Rossolini GM, Mangani S, Docquier JD. 2011.
698 Evolution to carbapenem-hydrolyzing activity in noncarbapenemase class D β-lactamase
699 OXA-10 by rational protein design. Proc Natl Acad Sci USA 108:18424–18429.
700 44. Huang TD, Poirel L, Bogaerts P, Berhin C, Nordmann P, Glupczynski Y. 2014. Temocillin and
701 piperacillin/tazobactam resistance by disc diffusion as antimicrobial surrogate markers for
702 the detection of carbapenemase-producing Enterobacteriaceae in geographical areas with
703 a high prevalence of OXA-48 producers. J Antimicrob Chemother 69:445-50.
704 45. Rima M, Emeraud C, Bonnin RA, Gonzalez C, Dortet L, Iorga BI, Oueslati S, Naas T. 2021.
705 Biochemical characterization of OXA-244, an emerging OXA-48 variant with reduced β-
706 lactam hydrolytic activity. J Antimicrob Chemother 76:2024-2028.

46. Emeraud C, Biez L, Girlich D, Jousset AB, Naas T, Bonnin RA, Dortet L. Screening of OXA-244 producers, a difficult-to-detect and emerging OXA-48 variant? J Antimicrob Chemother 75:2120-2123.
47. Paetzel M, Danel F, de Castro L, Mosimann SC, Page, MG, Strynadka NC. 2000. Crystal Structure of the Class D Beta-Lactamase OXA-10. Nat Struct Biol 7:918–925.
48. Dabos L, Bogaerts P, Bonnin RA, Zavala A, Sacré P, Iorga B, Huang DT, Glupczynski Y, Naas T. 2018. Genetic and Biochemical characterization of OXA-519, a novel OXA-48-like β-lactamase. Antimicrob Agents Chemother 62: e00469-18.
49. Kieser T. 1984. Factors affecting the isolation of CCC DNA from *Streptomyces lividans* and *Escherichia coli.* Plasmid 12:19–36.
50. Naas T, Sougakoff W, Casetta A, Nordmann P. 1998. Molecular characterization of OXA-20, a novel class D β-lactamase, and its integron from *Pseudomonas aeruginosa*. Antimicrob Agents Chemother 42:2074-2083.
51. Bradford MM. 1976. A rapid and sensitive method for the quantitation of microgram quantities of protein utilizing the principle of protein-dye binding. Anal Biochem 72:248–254.
52. Kabsch W. 2010. XDS. *Acta Crystallogr D Biol Crystallogr*. 66: 125-32.
53. Krug M, Weiss MS, Heinemann U, Mueller U .2012. XDSAPP: a graphical user interface for the convenient processing of diffraction data using XDS. J Appl Cryst 45:568-572.
54. French GS, Wilson KS. 1978. Acta. Cryst A 34:517.
55. Winn MD, Ballard CC, Cowtan KD, Dodson EJ, Emsley P, Evans PR, Keegan RM, Krissinel EB, Leslie AG, McCoy A, McNicholas SJ, Murshudov GN, Pannu NS, Potterton EA, Powell HR, Read RJ, Vagin A, Wilson KS. 2011. Overview of the CCP4 suite and current developments. Acta Crystallogr D Biol Crystallogr 67: 235-242.

731 56. Ten Eyck LF .1973. Crystallographic fast Fourier transforms. *Acta Cryst*. A29: 183-191.
732 57. McCoy AJ, Grosse-Kunstleve RW, Adams PD, Winn MD, Storoni LC, Read RJ. 2007. Phaser
733 crystallographic software. J Appl Crystallogr 40:658-674.
734 58. Read RJ, Adams PD, McCoy AJ. 2013. Intensity statistics in the presence of translational
735 noncrystallographic symmetry. Acta Crystallogr D Biol Crystallogr 69:176-83.
736 59. Kowiel M, Jaskolski M, Dauter Z .2014. ACHESYM: an algorithm and server for standardized
737 placement of macromolecular models in the unit cell. Acta Crystallogr D Biol Crystallogr
738 70:3290-3298.
739 60. Murshudov GN, Skubák P, Lebedev AA, Pannu NS, Steiner RA, Nicholls RA, Winn MD, Long
740 F, Vagin AA. 2011. REFMAC5 for the refinement of macromolecular crystal structures. Acta
741 Cryst D 67:355-367.
742 61. Emsley P, Lohkamp B, Scott WG, Cowtan K .2010. Features and development of Coot. *Acta*
743 *Crystallogr D Biol Crystallogr*. 66: 486-501.
744 62. Chen VB, Arendall WB, Headd JJ, Keedy DA, Immormino RM, Kapral GJ, Murray LW,
745 Richardson JS, Richardson DC. 2009. MolProbity: all-atom structure validation for
746 macromolecular crystallography. Acta Crystallogr D Biol Crystallogr 66:12-21.
747 63. Berman HM, Westbrook J, Feng Z, Gilliland G, Bhat TN, Weissig H, Shindyalov IN, Bourne
748 PE. 2000. The Protein Data Bank. Nucleic Acids Res 28:235-242.
749 64. DeLano WL .2014. The PyMOL Molecular Graphics System, version 1.7.0.0, Schrodinger,
750 LLC, New York.
751 65. Kleywegt GJ, Harris MR, Zou JY, Taylor TC, Wählby A, Jones TA. 2004. The Uppsala Electron-
752 Density Server. Acta Crystallogr D Biol Crystallogr 60:2240-2249.
753 66. Goddard TD, Huang CC, Meng EC, Pettersen EF, Couch GS, Morris JH, Ferrin TE. 2018. UCSF
754 ChimeraX: Meeting modern challenges in visualization and analysis. Protein Sci. 27: 14-25.

Table 1. MICs of β-lactam antibiotics for *K. pneumoniae* 1219, *E. coli* TOP 10 (pOXA-517), *E. coli* TOP 10 (pTOPO-OXA-48), *E. coli* TOP 10 (pTOPO-OXA-517), *E. coli* TOP 10 (pTOPO-OXA-405), *E. coli* TOP 10 (pTOPO-OXA-163), and *E. coli* TOP 10.

Antibiotic	MIC (µg/mL)					
	Kp 1219	*E. coli* TOP10				*E. coli* TOP10
		pOXA-517[a]	pTOPO-OXA-48	pTOPO-OXA-517[b]	pTOPO-OXA-163	
Amoxicillin	>256	>256	>256	>256	>256	2
Amoxicillin + CLA[c]	192	64	192	64	96	2
Piperacillin	>256	>256	128	>256	>256	1.5
Piperacillin + TZB[d]	96	96	12	96	32	1
Cefotaxime	>32	2	0.094	0.38	3	0.06
Ceftazidime	48	16	0.19	4	16	0.12
Ceftazidime+Avi[e]	1	1	0.5	0.5	ND	0.25
Cefepime	12	1	0.047	0.25	0.5	0.023
Imipenem	8	0.75	0.38	0.38	0.25	0.25
Meropenem	3	0.125	0.047	0.047	0.023	0.016
Ertapenem	3	0.125	0.047	0.047	0.032	0.003
Doripenem	3	0.094	0.094	0.094	0.023	0.06
Temocillin	192	192	>1024	32	32	4
Aztreonam	4	2	0.094	0.75	2	0.047

[a] natural plasmid carrying OXA-517
[b] recombinant pTOPO plasmids carrying OXA-48, OXA-517 and 0XA-163
[c] CLA, clavulanic acid (2 µg/mL)
[d] TZB, tazobactam (4 µg/mL)
[e] AVI: Avibactam (4 µg/mL)

Table 2. Kinetic parameters of OXA-48, OXA-517 and OXA-163, with representative β-lactam substrates.

	K_M (μM)			k_{cat} (s^{-1})			k_{cat}/K_M ($mM^{-1}s^{-1}$)		
Substrate	OXA-48	OXA-163	OXA-517	OXA-48	OXA-163	OXA-517	OXA-48	OXA-163	OXA-517
Ampicillin	395	315	226	955	23	58	2418	70	256
Oxacillin	95	90	48	130	34	30	1368	370	629
Temocillin	45	N.H.	729	0.30	N.H.	0.24	7	N.D.	0.32
Cefalotin	195	10	>1000	44	3	>59	226	300	38
Cefoxitin	>200	N.D	>1000	>0.05	N.D.	>6	0.26	N.D.	0.38
Ceftazidime	N.H.	>1000	>1000	N.H.	8	>20	N.D.	3	2
Cefotaxime	>900	45	>1000	>9	10	>22	10	230	16
Cefepime	>550	N.D.	>1000	>0.60	N.D.	>18	1.1	N.D.	11
Imipenem	13	520	411	5	0.03	6	369	0.06	14
Meropenem	11	>2000	>1000	0.07	0.10	>0.9	6	0.03	0.89
Ertapenem	100	130	>1000	0.13	0.05	>2.6	1.3	0.30	0.63
Aztreonam	N.H.	230	319	N.H.	0.50	1	N.D.	2	3.1

N.D., not determined. N.H., no detectable hydrolysis was observed with concentrations of substrate and enzymes up to 500 μM and 400 nM, respectively. Measurements were done in triplicate, and SD was within 10%

Data for OXA-48 are from Docquier *et al* (16). Data for OXA-163 are from Oueslati *et al* (5).

774 **Table 3**. X-ray data collection and structure refinement statistics

775

Data collection and processing	
Wavelength [Å]	0.98010
Resolution [Å]	46.37-1.86 (1.91-1.86)*
Space group	$P2_1$
Cell parameters [Å, º]	50.05/125.74/83.03/94.6
R_{meas} [%]	15.6 (125.3)
<I/σI>	6.57 (1.03)
$CC_{1/2}$ [%]	99.5 (34.7)
Completeness [%]	98.5 (91.9)
No. of unique reflections	84532 (13554)
Redundancy	3.3 (3.0)
Refinement	
R_{work} /R_{free}[%]	17.0/21.9
Rmsd bond lengths [Å]	0.012
Rmsd bond angles [º]	1.37
No. of protein molecules in ASU	4
No. of modeled amino acid residues	979
No. of all/protein/water/other atoms	8981/8072/738/185
Wilson B factor [$Å^2$]	24.2
Average B factor [$Å^2$] protein/water/other solvent/all	30.9/39.0/43.0/31.6
Ramachandran favored/allowed [%]	98/2
PDB code	6hb8

776 *Values in parentheses correspond to the highest resolution shell

777

Figure legends

Figure 1. (A) Nucleotide alignment of the β5-β6 loop region of the *bla*$_{OXA-48}$ and *bla*$_{OXA-517}$ genes (small letters). The corresponding amino-acid sequences of OXA-48 (3) and OXA-517 are shown in capital letters. **(B)** Alignment of the amino acid sequences of OXA-48 (3), OXA-163 (7) and OXA-517. For OXA-405 (8) and OXA-438 (10) only the β5-β6 loop is indicated. Asterisks indicate identical residues with OXA-48 AA sequence. Dashes indicate deleted amino acid residues. Amino acid motifs that are well conserved among class D β-lactamases are highlighted in gray. The β5-β6 loop sequence is boxed.

Figure 2. (A) Plasmid structures and genetic environments. Schematic representation of the genetic environments of the *bla*$_{OXA-48}$ (a), *bla*$_{OXA-405}$ (b), *bla*$_{OXA-517}$ (c), *bla*$_{OXA-163}$ (d), *bla*$_{OXA-247}$ (e), *bla*$_{OXA-181}$ (f), *bla*$_{OXA-232}$ (g), and *bla*$_{OXA-204}$ (h) genes. The Tn*1999* composite is formed by two copies of the IS*1999* insertion sequence, bracketing a fragment containing the *bla*$_{OXA-48}$, *bla*$_{OXA-405}$ and *bla*$_{OXA-517}$ genes. **(B)** Comparison of the major structural features of the plasmid pOXA-517 from *K. pneumoniae* 1219 with the prototype IncL *bla*$_{OXA-48}$ plasmid pOXA-48 (GenBank accession number JN626286) and pOXA-405. Common structures are highlighted in gray.

Figure 3. Cartoon model of a single subunit of OXA-517. The secondary structure elements are labeled according to (16). The model is colored by the B factor of the Cα atoms and the bar shows the color range in Å^2.

Figure 4. (A) An OXA-517 dimer shown as a cartoon model with two Arg206 residues and the bound sulfate ion shown as sticks. (**B)** A zoom-in view on the dimer interface with the partially occupied chloride (green sphere) and sulfate (red and yellow sticks) ions. Two equivalent arginine residues from the complementary subunits interact with the ions. This view is rotated 90° upwards compared to A. **(C)** The sulfate ion when modeled at full occupancy, in the 2mFo-DFc (blue,

contoured at 1.5σ) and mFo-DFc (+/-3.0σ, green/red) electron density maps, showing negative difference density. **(D)** The sulfate modeled at 0.5 occupancy with the electron density maps contoured at the same level as in C. A positive difference density peak is well visible, finally modeled as partial-occupancy Cl^- anion (green sphere in B).

Figure 5. (A) Alignment of the structures of OXA-517 (orange), OXA-48 (green) and OXA-163 (gray) showing variation in the length of the β5-β6 loop. **(B)** A close-up view of the backbone conformation of the loop with visible *cis*-peptide bonds preceding Pro217. Also visible is the difference in backbone conformation between OXA-163 (gray) and the other structures at Asp212. The distance between the Cα atoms of Arg214 (OXA-48) and Lys214 (OXA-517) is 3.8 Å. **(C)-(E)** Detailed views of the binding site in OXA-517 **(C)**, OXA-48 **(D)** and OXA-163 **(E)** with key residues rendered as sticks. All three figures have the same orientation.

Figure 6. (A) Superposition of the OXA-48 mutant P68A acyl-enzyme complex with ceftazidime structure (PDB id 6q5f, cyan) onto the native OXA-48 structure (PDB id 4s2p, green). Clashes shown as purple thick dashed lines. **(B)** Superposition of the OXA-48 mutant P68A acyl-enzyme complex with ceftazidime structure (PDB id 6q5f, cyan) onto the OXA-517 structure (orange). Clashes shown as purple thick dashed lines. All panels correspond to superposed structures viewed from the same distance and angle.

Figure 7. (A-C) Contacts between the β5-β6-loop residues and the residues previous to SER-70 α-helix or the Ω-loop residues in OXA-48 (PDB id 4s2p) **(A)**, OXA-517 (PDB id 6hb8) **(B)** and OXA-163 (PDB id 7khz) **(C)**. **(D)** Contacts between the residues before SER-70 α-helix and the Ω-loop residues in OXA-48 (PDB id 4s2p). Contacts are shown as purple thin dashed lines. Panels A, B, C correspond to superposed structures viewed from the same distance and angle.

A

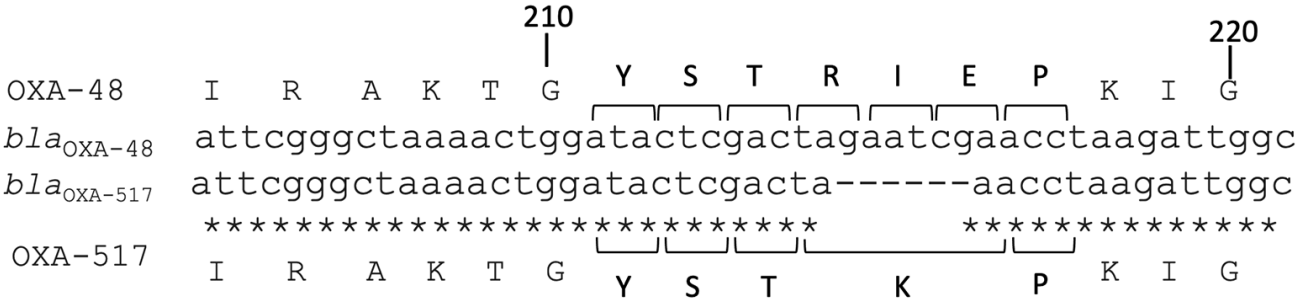
210
220
OXA-48
I R A K T G Y S T R I E P K I G
bla OXA-48
attcgggctaaaactggatactcgactagaatcgaacctaagattggc
bla OXA-517
attcgggctaaaactggatactcgacta------aacctaagattggc
OXA-517
I R A K T G Y S T K P K I G

B

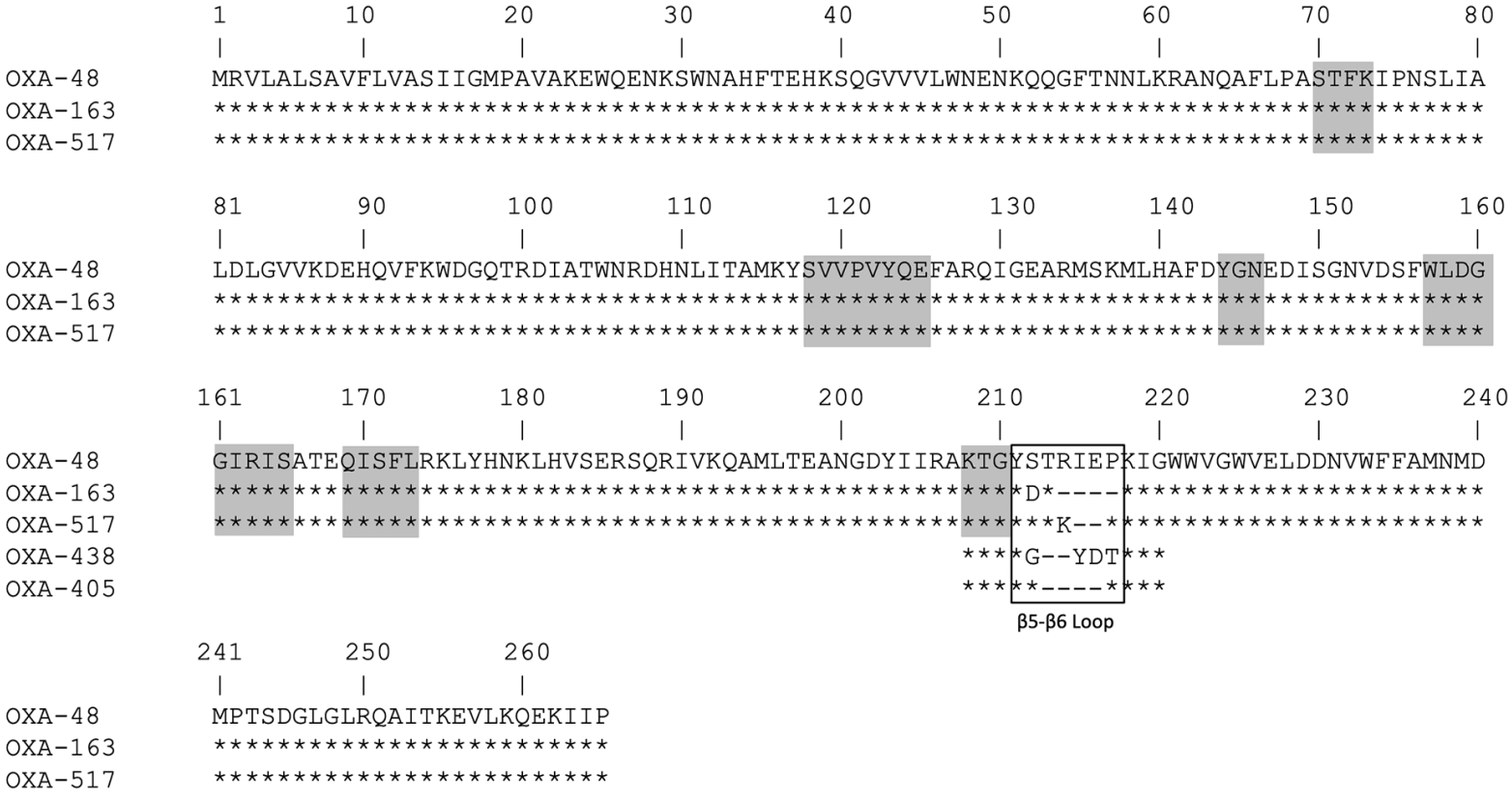
OXA-48
OXA-163
OXA-517
OXA-438
OXA-405
β5-β6 Loop

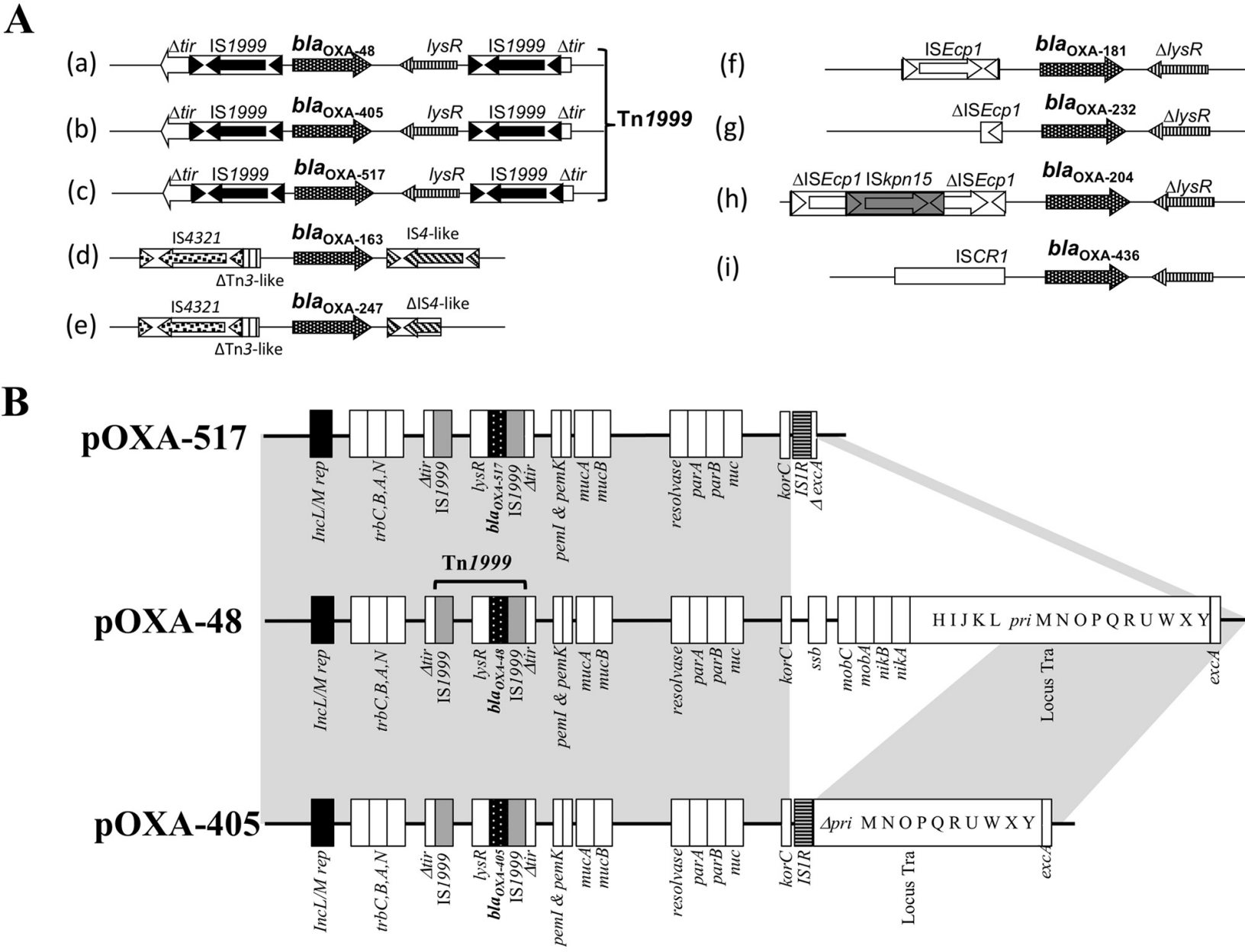
A
(a)
(b)
(c)
(d)
(e)
(f)
(g)
(h)
(i)
Δtir IS1999 blaOXA-48 lysR IS1999 Δtir
Δtir IS1999 blaOXA-405 lysR IS1999 Δtir
Δtir IS1999 blaOXA-517 lysR IS1999 Δtir
Tn1999
IS4321 blaOXA-163 IS4-like
ΔTn3-like
IS4321 blaOXA-247 ΔIS4-like
ΔTn3-like
ISEcp1 blaOXA-181 ΔlysR
ΔISEcp1 blaOXA-232 ΔlysR
ΔISEcp1 ISkpn15 ΔISEcp1 blaOXA-204 ΔlysR
ISCR1 blaOXA-436
B
pOXA-517
pOXA-48
pOXA-405
IncL/M rep
trbC,B,A,N
Δtir IS1999
lysR blaOXA-517 IS1999 Δtir
pemI & pemK
mucA mucB
resolvase parA parB nuc
korC ISIR Δ excA
Tn1999
lysR blaOXA-48 IS1999 Δtir
korC ssb
mobC mobA nikB nikA
H I J K L pri M N O P Q R U W X Y
Locus Tra
excA
lysR blaOXA-405 IS1999 Δtir
korC ISIR
Δpri M N O P Q R U W X Y

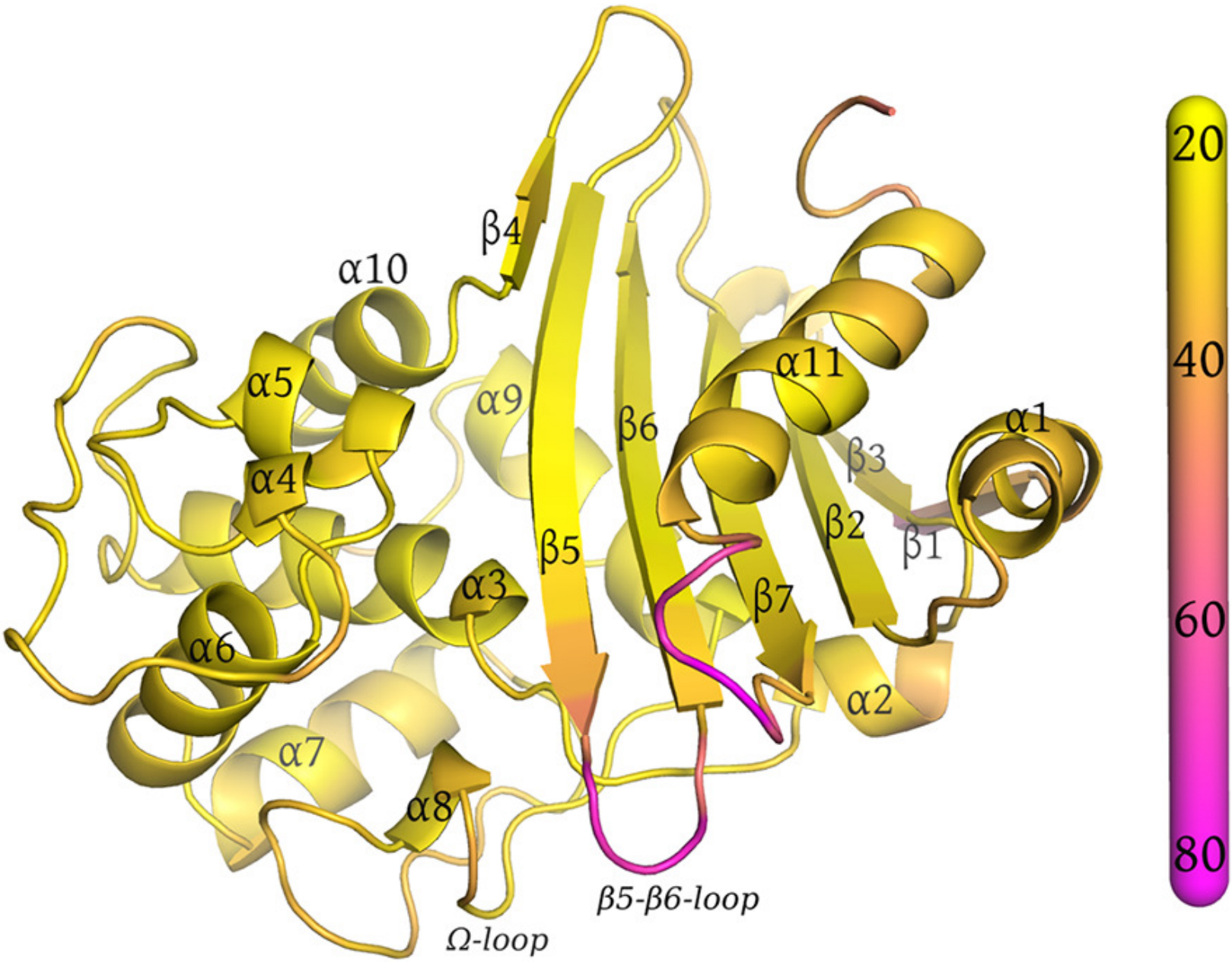
α10
β4
α5
α9
β6
α11
α1
α4
β3
β2
β1
β5
α3
β7
α6
α2
α7
α8
β5-β6-loop
Ω-loop
20
40
60
80

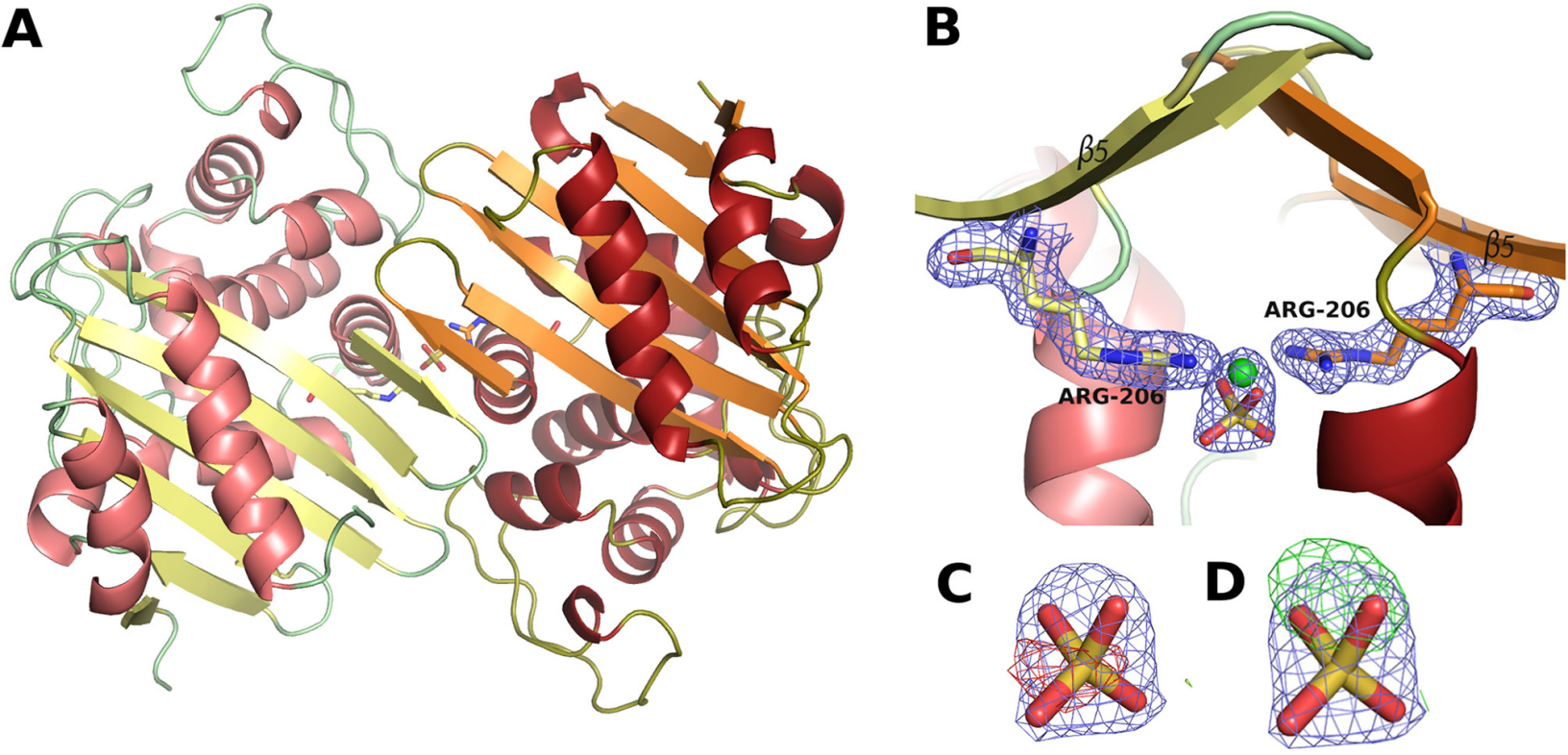
A
B
β5
β5
ARG-206
ARG-206
C
D

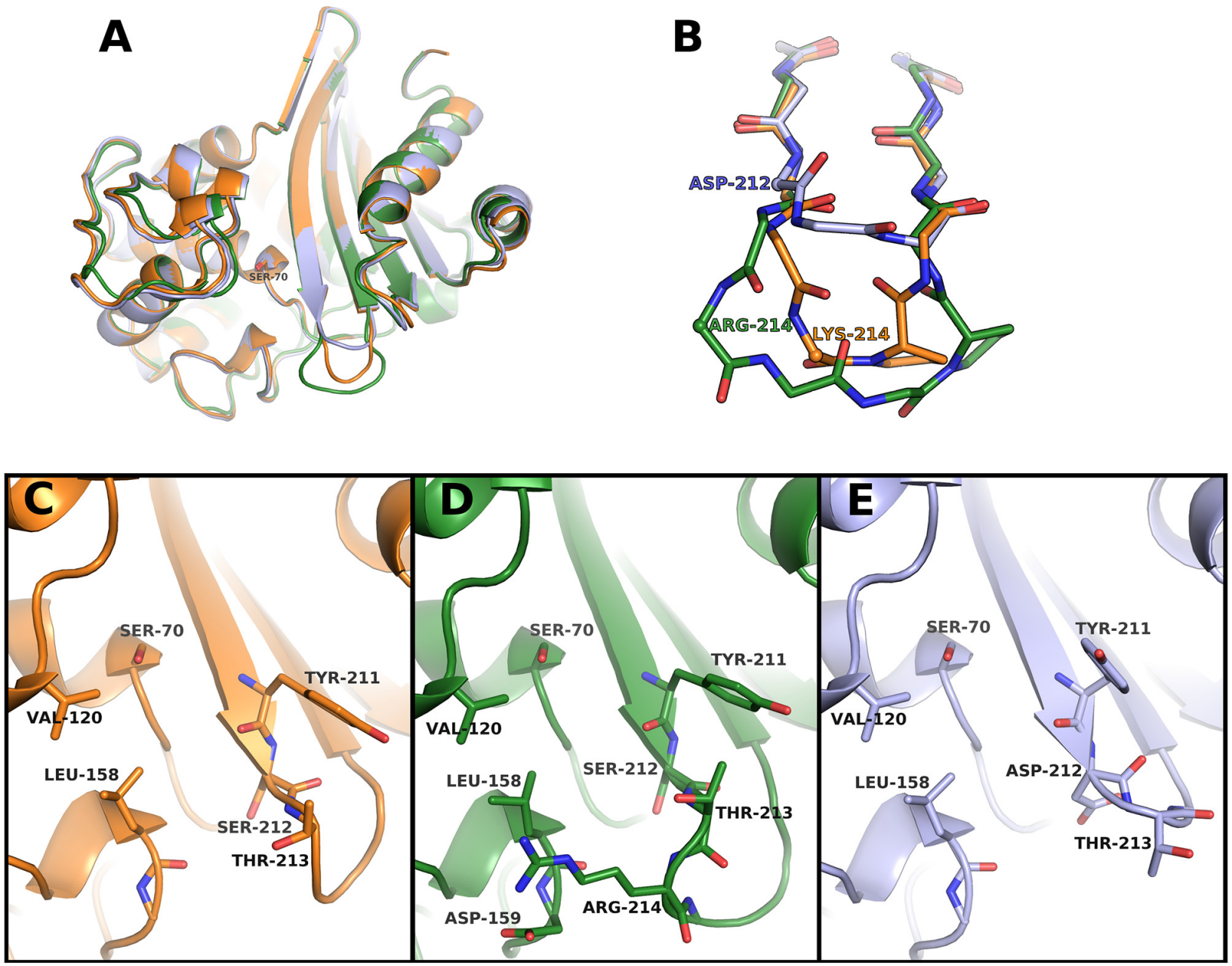
A
SER-70
B
ASP-212
ARG-214
LYS-214
C
SER-70
TYR-211
VAL-120
LEU-158
SER-212
THR-213
D
SER-70
TYR-211
VAL-120
SER-212
LEU-158
THR-213
ASP-159
ARG-214
E
SER-70
TYR-211
VAL-120
LEU-158
ASP-212
THR-213

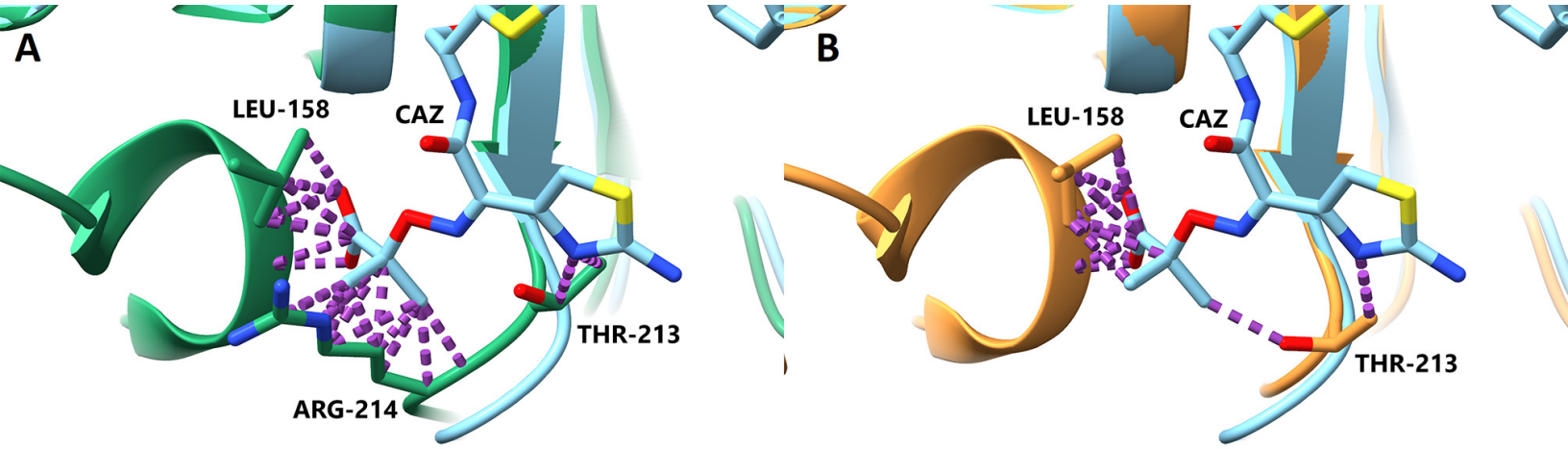
A
LEU-158
CAZ
THR-213
ARG-214
B
LEU-158
CAZ
THR-213

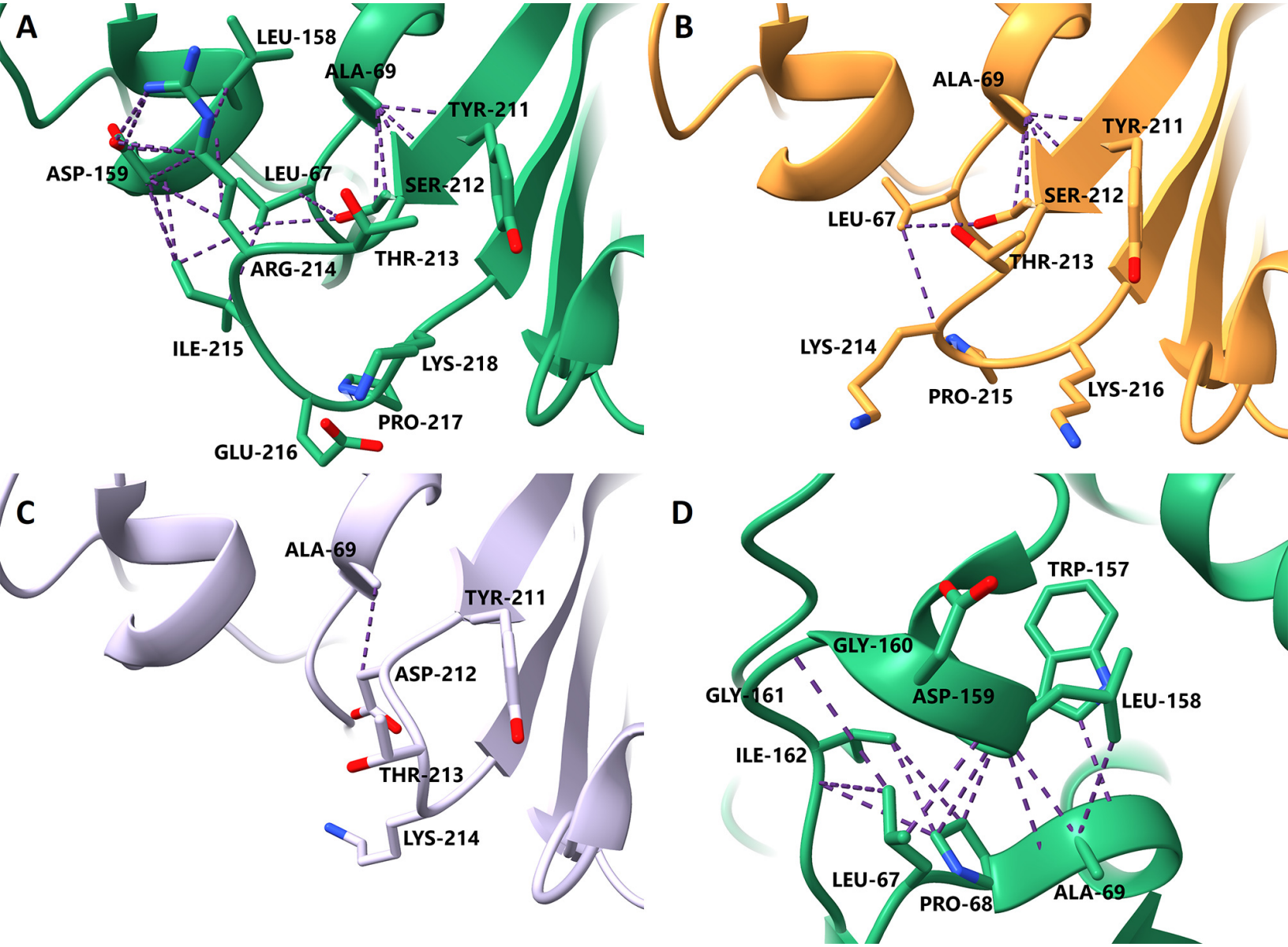
A
LEU-158
ALA-69
TYR-211
ASP-159
LEU-67
SER-212
THR-213
ARG-214
ILE-215
LYS-218
PRO-217
GLU-216
B
ALA-69
TYR-211
SER-212
LEU-67
THR-213
LYS-214
PRO-215
LYS-216
C
ALA-69
TYR-211
ASP-212
THR-213
LYS-214
D
TRP-157
GLY-160
GLY-161
ASP-159
LEU-158
ILE-162
LEU-67
PRO-68
ALA-69

Supplementary material

Structural and biochemical features of OXA-517: a carbapenem and expanded-spectrum cephalosporin hydrolyzing OXA-48 variant**.**

Laura Dabos[1,2], Joanna E. Raczynska[3], Pierre Bogaerts[5], Agustin Zavala[6], Delphine Girlich[1,2], Remy A. Bonnin[1,2], Laurent Dortet[1,2], Aurélie Peyrat[1], Pascal Retailleau[6], Bogdan I. Iorga[6], Mariusz Jaskólski[3,7], Youri Glupczynski[5], Thierry Naas[1,2,4*]

[1] Team "Resist" UMR1184 "Immunology of Viral, Auto-immune, Hematological and Bacterial diseases (IMVA-HB), INSERM, University Paris-Saclay, LabEx LERMIT, Faculty of Medicine, Le Kremlin-Bicêtre, France.

[2] French National Reference Center for Antibiotic Resistance: Carbapenemase-producing Enterobacteriaceae, Le Kremlin-Bicêtre, France:

[3] Center for Biocrystallographic Research, Institute of Bioorganic Chemistry, Polish Academy of Sciences, Poznan, Poland.

[4] Department of Bacteriology-Hygiene, Bicêtre Hospital, APHP Paris-Saclay, Le Kremlin-Bicêtre, France

[5] Laboratory of clinical microbiology, National reference center for monitoring antimicrobial resistance in Gram-negative bacteria, CHU UCL Namur, Yvoir, Belgium.

[6] Université Paris-Saclay, CNRS UPR 2301, Institut de Chimie des Substances Naturelles, Labex LERMIT, Gif-sur-Yvette, France.

[7] Department of Crystallography, Faculty of Chemistry, A. Mickiewicz University, Poznan, Poland.

Clinical case

Figure S1 and S2

Clinical Case

K. pneumoniae 1219 clinical isolate (*Kp* 1219) was recovered from culture of a sputum specimen of 81-year-old women hospitalized in a Belgium hospital for rapid alteration of general status, fever (39°C) and lumbar pain shown to be associated with a hydro-ureteronephrosis due to an obstructive renal stone for which stenting of the left ureteral orifice was performed in the operative room on the next day. Blood and urine cultures obtained on admission revealed the presence of a *Proteus mirabilis* (wild-type susceptible to all antibiotics). Antimicrobial therapy was initiated with temocillin (2 g/IV bid) and rapidly switched to piperacillin 4 g/IV qid because of rapid alteration of the status and development of a severe septic shock (thrombocytopenia, 3.000 platelets/mm^3) with acute renal failure (estimated GFR (glomerular filtration rate) of 21 ml/min). The patient had to be admitted to the intensive care unit where she received high dose of vasopressor drugs (norepinephrine 1 µg/kg/min) and was intubated and mechanically ventilated. Her stay was complicated by the development of a right lower lobe ventilator-associated pneumonia episode for which she was treated with several antimicrobial agents including meropenem (1g/IV tid) followed by cefepime (2g/IV tid), colistin (4.5 million units/bid after a loading dose of 9 million units) and tigecycline (100 mg/IV bid). She then developed an acute infectious enterocolitis with active gross bleeding due to *Clostridium difficile* for which she was treated by metronidazole (500 mg tid) and vancomycin (250 mg qid) per os. The patient was nursed in single isolation room during the remaining duration of her ICU stay. After four weeks, she was transferred to another unit for palliative care and eventually died shortly after *Kp* 1219 isolate was repeatedly isolated over the period from throat, sputum, tracheobronchial aspirates and BAL (bronchoalveolar lavage) specimens of the patient.

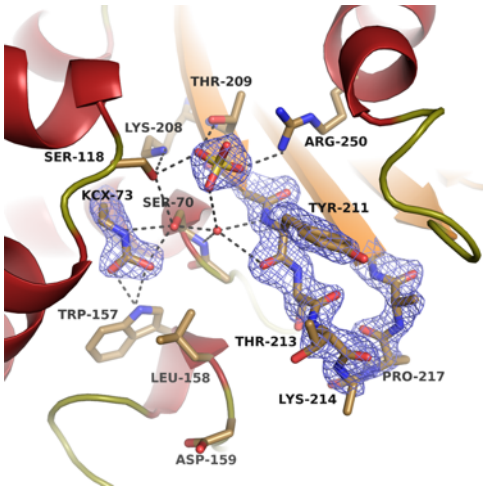

Figure S1. The active site of OXA-517 with residues implicated in substrate binding and the hydrolysis reaction shown as sticks. The only water molecule (small red sphere) in the active site that is preserved in all four protein subunits in the crystal is bound in the oxyanion hole. 2mFo-DFc electron density (contoured at 1σ) is shown for the carboxylated lysine residue (Kcx73), the sulfate ion and the residues in loop β5-β6.

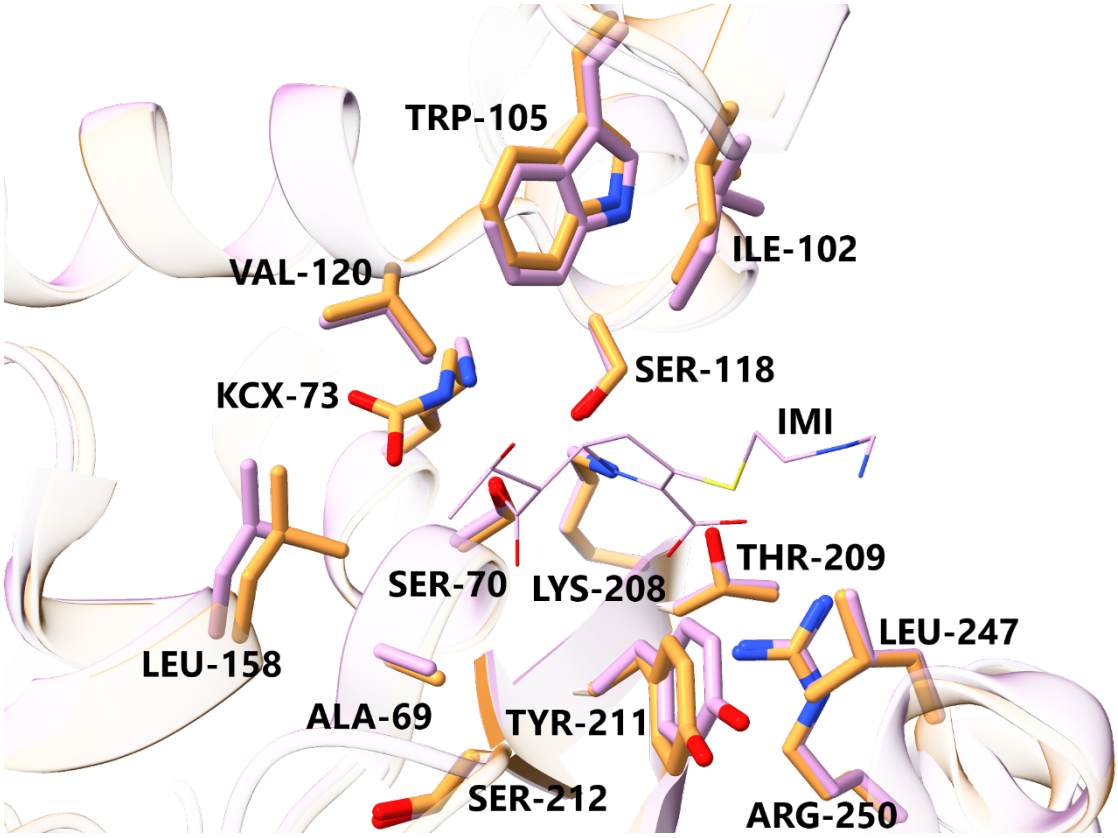

Figure S2. Superposition of OXA-48 acyl-enzyme complex with imipenem structure (PDB id 6p97, pink) onto the OXA-517 structure (PDB id 6hB8, orange). Residues surrounding imipenem are shown as thick sticks. Imipenem is shown as thin sticks, to allow a clearer view of surrounding residues potentially blocked by it.